Received: Added at production | Revised: Added at production | Accepted: Added at production

DOI: xxx/xxxx

ARTICLE TYPE

In silico study of vessel and stent-graft parameters on the potential success of endovascular aneurysm repair

André Hemmler[1] | Brigitta Lutz[2] | Christian Reeps[2] | Michael W. Gee[1]

[1]Mechanics & High Performance Computing Group, Technische Universität München, Parkring 35, 85748 Garching b. München, Germany

[2]Klinik für Viszeral-, Thorax- und Gefäßchirurgie, Universitätsklinikum Carl Gustav Carus Dresden, Fetscherstraße 74, 01307 Dresden, Germany

Correspondence
Michael W. Gee, Mechanics & High Performance Computing Group, Technische Universität München, 85748 Garching b. München, Germany. Email: gee@tum.de

Summary

The variety of stent-graft (SG) design variables (e.g. SG type and degree of SG oversizing) and the complexity of decision making whether a patient is suitable for endovascular aneurysm repair (EVAR) raise the need for the development of predictive tools to assist clinicians in the preinterventional planning phase. Recently, some in silico EVAR methods have been developed to predict the deployed SG configuration. However, only few studies investigated how to assess the in silico EVAR outcome with respect to EVAR complication likelihoods (e.g. endoleaks and SG migration).

Based on a large literature study, in this contribution, 20 mechanical and geometrical parameters (e.g. SG drag force and SG fixation force) are defined to evaluate the quality of the in silico EVAR outcome. For a cohort of n=146 realizations of parameterized vessel and SG geometries the in silico EVAR results are studied with respect to these mechanical and geometrical parameters. All degrees of SG oversizing in the range between 5% and 40% are investigated continuously by a computationally efficient parameter continuation approach.

The in silico investigations have shown that the mechanical and geometrical parameters are able to indicate candidates at high risk of postinterventional complications. Hence, this study provides the basis for the development of a simulation based metric to assess the potential success of EVAR based on engineering parameters.

KEYWORDS:
abdominal aortic aneurysm, endovascular repair, stent-graft, hostile neck, oversizing

1 | INTRODUCTION

Endovascular aneurysm repair (EVAR) requires stent-graft (SG) devices that interact perfectly with the vessel such that the aneurysm sac is permanently excluded from the main blood flow and the abdominal aortic aneurysm (AAA) is prevented from rupture. Especially in case of unfavorable vessel morphologies, EVAR might fail or lead to possible secondary interventions. In contrast, EVAR is considered to be successful if the aneurysm stays excluded and has no expansion for several years after the intervention. Reasons for immediate or long-term failure of EVAR are difficult to identify, but both wrong SG sizing[89,16,42,86] and inappropriate vessel morphologies[78,93,22] are frequent explanations in literature. Device manufacturers formulate the limits of applicability of EVAR in their instructions for use (IFU)[78,58] which state for instance that the aortic neck should not exceed a certain angle and that the neck requires a certain minimum length. From an engineering perspective, the IFU should

not be formulated in terms of geometrical preinterventional parameters (e.g. neck angle) but rather in terms of mechanical and geometrical postinterventional parameters which predict the quality of the EVAR outcome and hence predict the success of the EVAR procedure. In silico EVAR methodologies are able to make predictions of the deployed state under realistic conditions[32,64,5]. However, the major question of how to evaluate the in silico results with respect to the quality of the EVAR outcome still is largely unsolved. This aspect raises the claim for the definition of a set of mechanical and geometrical parameters (e.g. SG drag force[46,24,59], SG fixation force[32,55], tissue stresses[2,32,33,40] and the quality of seal[3,74]) to assess the quality of the in silico EVAR outcome and their validation of being able to indicate EVAR related complications (e.g. endoleaks[28,12], SG migration[89,86,2], stress induced aortic neck dilatation[41,89] and SG fracture[40,6]). This bridging of the gap between predictive in silico EVAR methodologies and interpretation of the potential success of EVAR is the next step towards the usage of in silico EVAR approaches in clinical practice. In clinical practice, a simulation needs to be easily understandable for the clinician and reliable to predict the complication likelihoods of EVAR for patient-specific cases.

The objective of this study is to investigate the influence of the vessel morphology and the SG geometry on EVAR outcomes from a mechanical and engineering perspective. The definition of parameterized vessels and SGs enables large cohort statistical investigations. For the assessment of the quality of the in silico EVAR outcome, suitable mechanical and geometrical parameters are defined based on a comprehensive literature study. These parameters are denoted as *EVAR quality parameters* in the following. Furthermore, the impacts of specific parameters, such as the influence of the degree of SG oversizing, the influence of patient-specific vessel uncertainties[7], the influence of aortic neck calcification and the influence of the aortic blood pressure state on the quality of the in silico EVAR outcome is investigated in this study.

A large parameter study of parameterized vessels and SGs might help to give answers to open question such as the best value for SG oversizing[89,10] depending on the morphology of the vessel. Further, it might provide clarification on specific questions such as whether excessive SG oversizing can compensate the drawbacks of EVAR in unfavorable aortic morphologies. This hypothesis is presumed by Van Keulen et al.[88] whereas Canaud et al.[10] report adverse effects of excessive SG oversizing especially in unfavorable aortic morphologies such as large neck angles.

In silico EVAR is a challenging and highly complex problem including numerically difficult contact interactions between SG and vessel as well as strong buckling of the membranous graft. These aspects make in silico EVAR approaches computationally very expensive. Hence, a large parameter study requires numerical techniques to increase the efficiency and to reduce computational costs. Vessel morphologies and SG shapes can be very diverse and complex. Finding a parameterization of these objects which is able to reproduce a wide range of realistic vessel and SG geometries and whose parameters can be related to the parameters in the IFU is challenging.

In this study, we propose a full parameterization of an AAA by 16 parameters. Further, a full parameterization of a SG by 7 parameters is used. The deployed state of the elastically deformable SG in a hyperelastic, anisotropic vessel with consideration of intraluminal thrombus (ILT) and calcifications is approximated by the in silico EVAR methodology proposed by our group[32]. We apply sophisticated models of SG and vessel which consider stent predeformation[32,75] and vessel prestressing[27]. In total, we perform 146 in silico EVAR simulations of 146 different realizations of the parameters of the vessel and the SG. The degree of SG oversizing is investigated continuously in the range between 5% to 40% in a computationally efficient way. To demonstrate the clinical relevance and to prove the applicability of the presented methods to patient-specific data, we evaluate the EVAR quality parameters for 4 patient-specific cases and compare the results of the EVAR quality parameters to the ones obtained from the parameter study with the synthetic vessel geometry.

Some studies have already been conducted to evaluate the influence of vessel and SG parameters on EVAR outcomes based on in silico approaches (e.g.[18,65,2,3,70,66,67]). Most of these studies used only a very limited number of EVAR quality parameters and a very limited number of variations of the vessel and SG geometry. Polanczyk et al.[66,67] used a parameterization of bifurcated SGs to assess the postinterventional hemodynamics and simulate thrombus formation in the SG by application of computational fluid dynamic simulations. De Bock et al.[18] varied the neck angle, the SG position and the degree of SG oversizing in a full factorial analysis of in total 72 simulations in an angulated tube-shaped vessel with linear elastic material properties and without consideration of ILT and calcifications. To asses the quality of the EVAR outcome, they defined 4 EVAR quality parameters. Perrin et al.[65] used finite element analysis to simulate the expansion of five marketed SGs in an idealized aneurysm and to evaluate quantitatively their mechanical performances. Altnji et al.[2,3] performed a small parameter study in a patient-specific thoracic aneurysm geometry with respect to stent design parameters and their impact on SG migration. However, rather strong simplifications were used, such as neglecting the graft.

This paper is structured as follows: in Section 2, we state the basic modeling approaches, define a full parameterization of vessel and SG, give a large summary of EVAR quality parameters to estimate the quality of the in silico EVAR outcome and

describe the framework of the proposed parameter study. In Section 3, we evaluate the results of the parameter study statistically, quantitatively and qualitatively. The discussion of these findings is done in Section 4. Finally, limitations and conclusions of this study are provided in Section 5 and 6, respectively.

2 | MATERIALS AND METHODS

2.1 | Computational Modeling

We apply the in silico EVAR methodology presented in [32] to approximate the deployed configuration of the elastic SG in the elastically deformable vessel under physiologically meaningful but static conditions. Mortar based mesh tying [68] is used to model the attachment between stent and graft. Mortar based frictional contact [68] with a friction coefficient of $\mu = 0.4$ [64] and a penalty regularization of the contact constraints is applied between SG outer surface and the luminal vessel surface. A modified updated Lagrangian formulation [27] is used to prestress the vessel to the diastolic pressure of $p^{\text{diast}} = 80$ mmHg. The hyperelastic constitutive models and material parameters of vessel wall, ILT, calcifications, stent and graft are taken from [32] and are summarized in Appendix A1. Constitutive SG parameters are chosen to be in the range of marketed SGs with ePTFE graft and stainless steel stent [40,20]. Spring boundary conditions with a spring stiffness of 2.0 kPa/mm [57] on the abluminal vessel wall boundary are used to model the surrounding tissue of the abdominal aorta.

As the constitutive model of the vessel wall has a distinct influence on the definition of some EVAR quality parameters that will be introduced in section 2.4, we briefly repeat the definition of this kind of strain energy function (SEF) taken from [32]. The SEF of the vessel wall

$$\Psi^{\text{wall}} = (1 - \lambda(d))\Psi^{\text{AA}} + \lambda(d)\Psi^{\text{AAA}} \tag{1}$$

incorporates a smooth blend between "healthy" ($\lambda = 0$) and "aneurysmatic" ($\lambda = 1$) aortic wall where the blend parameter $\lambda(d) \in [0; 1]$ is a function of the local vessel diameter d, Ψ^{AA} is the anisotropic SEF of the "healthy" aortic wall according to [25] and Ψ^{AAA} is the isotropic SEF of the "aneurysmatic" aortic wall according to [73]. Consequently, in regions of $\lambda = 0$ the constitutive behavior of the vessel wall is fully governed by the "healthy" SEF Ψ^{AA}, in regions of $\lambda = 1$ the constitutive behavior of the vessel wall is fully governed by the "aneurysmatic" SEF Ψ^{AAA} and in-between, i.e. $\lambda = (0; 1)$, a transition zone exists. In this transition zone, the constitutive behavior of the vessel wall is interpolated between the "healthy" SEF Ψ^{AA} and the "aneurysmatic" SEF Ψ^{AAA}.

The vessel geometries are discretized using a conforming and hexahedron-dominated mesh with F-bar-based element technology [19]. The stent is discretized by linear, hexahedral elements with enhanced assumed strain (EAS) technology whereas the graft is meshed by hexahedral solid-shell elements [91] with EAS and assumed natural strain (ANS) technology similar to the discretization techniques described in [32]. The proposed discretizations of vessel and SG result on average in approximately 400.000 degrees of freedom. A mesh convergence study is provided in Appendix A2. All simulations are performed using an in-house nonlinear finite element code.

2.2 | Vessel parameterization

Although most EVAR related complications are associated with inappropriate conditions at the aortic neck, we use a realistic representation of the total AAA due to two main reasons. First, some EVAR quality parameters, such as the SG drag force and the mean diametric graft compliance, require the consideration of the total aorta covered by the SG and not only the neck region. Second, all methods proposed in this study shall be applicable to real, patient-specific cases. Nevertheless, to reduce the complexity of the vessel and SG parameterizations we restrict this study to an AAA and a SG without bifurcation to the iliac arteries. Both, the vessel and the SG model are generated in Trelis 15.1 (Csimsoft, Utah) in a fully automatic manner using its Python interface.

We use a parameterized vessel that is rotationally symmetric around the plane and smooth curve $C(s) \subset \mathbb{R}^2$, which is a higher order spline (Trelis 15.1, Csimsoft, Utah) in the global XY-plane through the five points E_p, S_p, O, S_d, E_d according to Figure 1I. The locations of the five points are defined by the seven parameters: proximal neck angle α_p, distal neck angle α_d, proximal neck length l_p, distal neck length l_d, proximal eccentricity e_p, distal eccentricity e_d and aneurysm length l_{AAA}. Further, the three-dimensional representation of the vessel is defined by the six parameters: proximal neck diameters d_p, distal neck diameter d_d, AAA diameter d_{AAA}, proximal shoulder length l_{sp}, distal shoulder length l_{sd}, vessel wall thickness t_w and maximal thickness t_{ILT}

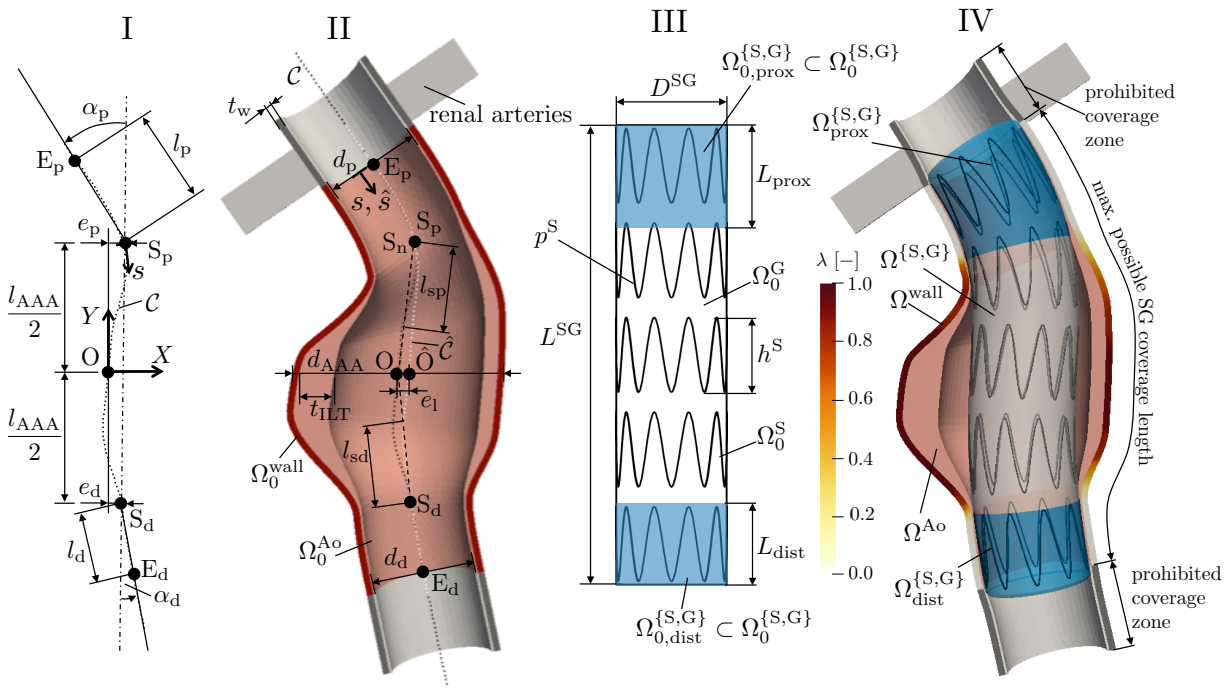

FIGURE 1 Definition of the curve $\mathcal{C}(s)$ through the five points E_p, S_p, O, S_d and E_d (I). Definition of the curve $\hat{\mathcal{C}}(\hat{s})$ through the five points E_p, S_p, $\hat{O}$, S_d and E_d and 3D geometry of the parameterized vessel (II) (renal arteries are not part of the computational model). Geometry of the parameterized SG and visualization of the proximal and distal landing zones (blue) of length L_{prox} and L_{dist}, respectively (III). Placed SG with proximal position below the bifurcation to the renal arteries and visualization of the blending parameter λ to smoothly blend between "healthy" and "aneurysmatic" aortic wall (IV). Definition of domains in the reference configuration Ω_0 and in the current configuration Ω.

of the ILT. The proximal shoulder length l_{sp} and the distal shoulder length l_{sd} define the length of the transition zone between the diameter of the "aneurysmatic" vessel and the "healthy" vessel in the neck and the distal part, respectively.

The luminal region is rotationally symmetric around the plane curve $\hat{\mathcal{C}}(\hat{s}) \subset \mathbb{R}^2$ through the five points E_p, S_p, $\hat{O}$, S_d, E_d according to Figure 1II where the point $\hat{O}$ is shifted by the eccentricity e_l with respect to the point O (Figure 1). The eccentricity e_l of the luminal centerline is implicitly given by

$$e_l = l_{AAA}\left(\mathrm{sgn}\,(\alpha_p)\kappa_p - \mathrm{sgn}\,(\alpha_d)\kappa_d\right) \tag{2}$$

where sgn(•) is the sign function and $\kappa_p = ||\frac{d^2C}{ds^2}(s = S_p)||$ as well as $\kappa_d = ||\frac{d^2C}{ds^2}(s = S_d)||$ are the curvatures of the curve $\mathcal{C}$ at the points S_p and S_d, respectively. The heuristic definition of e_l in equation (2) is motivated by the fact, that the ILT thickness generally is larger at the flow averted side than at the flow faced side.

Spots of calcified tissue are considered in the domain of the vessel Ω_0^{Ao} according to[32]. To assess the degree of calcification, we introduce the percentage circumferential proximal neck calcification $\bar{c}_{prox}^{Ao}$ which is the ratio of the luminal surface in the proximal landing zone of the vessel covered by calcifications and the total luminal vessel surface of the proximal landing zone.

Vessel uncertainties[7] (e.g. the vessel wall thickness t_w and the vessel wall stiffness) are quantities of the vessel model that are usually not easy to obtain and which are mostly incorporated in terms of population-averaged quantities. To investigate the impact of the vessel wall stiffness in a strongly simplified manner, we define the scaled SEF of the vessel wall

$$\tilde{\Psi}^{wall} = \gamma \Psi^{wall} \tag{3}$$

where γ is a scalar valued scaling parameter. γ is spatially constant for any $\boldsymbol{X} \in \Omega_0^{wall}$, i.e. intrapatient variability of γ is not considered.

In total, we define the set $\mathcal{G}^{Ao} = [\alpha_p, \alpha_d, l_p, l_d, e_p, e_d, l_{AAA}, d_p, d_d, d_{AAA}, l_{sp}, l_{sd}, t_w, t_{ILT}, \bar{c}_{prox}^{Ao}, \gamma]$ which uniquely describes the vessel model with an AAA by 16 parameters $g^{Ao} \in \mathcal{G}^{Ao}$ as visualized in Figure 1I+II.

2.3 | Stent-graft parameterization

In clinical practice, the length of a SG generally is chosen as long as possible to obtain relatively long landing zones at the proximal and distal ends where the maximum length in the given problem is limited by the renal arteries at the proximal end. For simplicity, we consider an AAA without bifurcation to the iliac arteries. Further, the renal arteries are not part of the computational model. However, the points $\mathrm{E_p}$ and $\mathrm{E_d}$ define the locations of the renal arteries and the bifurcation of the iliac arteries, respectively (Figure 1II+IV). Therefore, in the model the location of the two points $\mathrm{E_p}$ and $\mathrm{E_d}$ define the maximal possible coverage length of the SG (Figure 1IV). The aorta proximal of the point $\mathrm{E_p}$ and distal of the point $\mathrm{E_d}$ must not be covered by the SG as this would occlude the renal arteries and parts of the iliac arteries, respectively. Under the assumption that the maximal possible coverage length of the SG is used, the length L^{SG} of the SG is implicitly given by the length of the luminal vessel centerline $\hat{C}$ between the two points $\mathrm{E_p}$ and $\mathrm{E_d}$ (Figure 1II):

$$L^{\mathrm{SG}} = \int_{\mathrm{E_p}}^{\mathrm{E_d}} \mathrm{d}\hat{s} = \int_{Y_{\mathrm{E_p}}}^{Y_{\mathrm{E_d}}} \sqrt{1 + \left(\frac{\mathrm{d}X_{\hat{C}}}{\mathrm{d}Y_{\hat{C}}}\right)^2}\, \mathrm{d}Y_{\hat{C}}. \tag{4}$$

$X_{\hat{C}}$ and $Y_{\hat{C}}$ are the coordinates of the curve $\hat{C}$ in the XY-plane.

We define the nominal degree of SG oversizing as the ratio between the nominal diameter D^{SG} of the SG and the inner vessel wall diameter d_{p} in the aortic neck:

$$o = \frac{D^{\mathrm{SG}}}{d_{\mathrm{p}}} - 1. \tag{5}$$

Consequently, for a given degree of SG oversizing, the nominal diameter of the SG is implicitly given by

$$D^{\mathrm{SG}} = (o + 1)d_{\mathrm{p}}. \tag{6}$$

Most marketed SGs are manufactured with a stent diameter D^{S} larger than the associated graft diameter. During the assembling process of stent and graft, the stent rings are radially compressed resulting in an assembled SG with residual strains and stresses. This effect, known as stent predeformation[32,75], has to be considered in an in silico EVAR simulation. The degree of stent predeformation ω is defined by the ratio of the stress-free diameter D^{S} of the stent, i.e. the diameter of the stent before the assembly of stent and graft, and the nominal diameter D^{SG} of the SG:

$$\omega = \frac{D^{\mathrm{S}}}{D^{\mathrm{SG}}} - 1. \tag{7}$$

The shape of each stent limb is defined by

$$\boldsymbol{X}^{\mathrm{S}} = \begin{pmatrix} \frac{D^{\mathrm{S}}}{2}\cos(\varphi) \\ \frac{D^{\mathrm{S}}}{2}\sin(\varphi) \\ \frac{h^{\mathrm{S}}}{2}\sin(\varphi p^{\mathrm{S}}) \end{pmatrix}, \quad \varphi \in [0; 2\pi], \tag{8}$$

where h^{S} is the height of the stent limb and p^{S} is the number of sinusoidal periods per stent limb. All n^{S} stent limbs are equally distributed along the graft length. Graft thickness of $t^{\mathrm{G}} = 0.05$ mm and thickness of $t^{\mathrm{S}} = 0.33$ mm of the stent wires with quadratic cross section are chosen to be in the range of marketed SGs[20] and are not modified in this study.

In total, we define the set $\mathcal{G}^{\mathrm{SG}} = [h^{\mathrm{S}}, p^{\mathrm{S}}, n^{\mathrm{S}}, \omega, t^{\mathrm{G}}, t^{\mathrm{S}}]$ which uniquely (uniquely with exception of its diameter D^{SG}) describes the geometry of the SG in the preinterventional configuration $\Omega_0^{\mathrm{SG}} = \Omega_0^{\mathrm{S}} \cup \Omega_0^{\mathrm{G}}$ by 6 parameters $g^{\mathrm{SG}} \in \mathcal{G}^{\mathrm{SG}}$ (Figure 1III). In contrast to the discrete parameters $g \in \mathcal{G} = \mathcal{G}^{\mathrm{Ao}} \cup \mathcal{G}^{\mathrm{SG}}$, the degree of SG oversizing $o(D^{\mathrm{SG}})$, which implicitly defines the nominal diameter of the SG (equation (6)), is treated as continuous parameter by a SG parameter continuation approach described in Section 2.5.

2.4 | Definition of EVAR quality parameters and their impact on EVAR related complications

In this section, we define mechanical and geometrical parameters to estimate the quality of the EVAR outcome. These parameters will be denoted as *EVAR quality parameters* $q \in \mathcal{Q}$. We do not evaluate medical, biological or other parameters that also might have an influence on the quality of the EVAR outcome. The EVAR quality parameters have to satisfy the following basic demands:

TABLE 1 Summary of all EVAR quality parameters $q \in \mathcal{Q}$ and their potential influence on the EVAR outcome.

	EVAR quality parameter	Reference	Symbol [dimension]	Equation	Potential influence[b]	Associated complications
Tractions / stresses	Max. vessel stress	2,32,33,40,39	$\sigma_{99}^{\text{wall}}$ [kPa]	-	↓	Aortic neck dilatation
	Max. vessel overstress		$\bar{\sigma}_{99}^{\text{wall}}$ [kPa]	(13)	↓	
	Max. vessel relief[a]	-	$\lvert\bar{\sigma}_{1}^{\lambda,\text{wall}}\rvert$ [kPa]	(14)	↑	
	Max. aneurysmatic overstress[a]		$\bar{\sigma}_{99}^{\lambda,\text{wall}}$ [kPa]	(14)	↓	
	Max. normal contact traction	2,3,39	$t_{\text{n},99}$ [kPa]	(15)	↓	
	Max. stent stress	2,3,40	σ_{99}^{S} [GPa]	-	↓	SG fatigue
Fixation / drag forces	Proximal fixation force	[32 3,55,42,72][d]	$\hat{F}_{\text{prox}}$ [N]	(17)	↑	SG migration
	Distal fixation force		$\hat{F}_{\text{dist}}$ [N]	(17)	↑	
	Lateral drag force	85,46,24,59,38,15	$F_{\text{drag,x}}$ [N]	(16)	↓	
	Axial drag force		$F_{\text{drag,y}}$ [N]	(16)	↓	
Quality of seal	Proximal fixation area	3,80	$a_{\text{prox}}^{\text{seal}}$ [mm^2]	(18)	↑	Endoleak type I
	Proximal max. graft-vessel distance	74,18	$s_{\text{max}}^{\text{GA}}$ [mm]	(19)	↓	
	Proximal max. stent-vessel distance		$s_{\text{max}}^{\text{SA}}$ [mm]	(20)	↓	
SG geometry	Effective SG oversizing	[89][c]	$\bar{o}_{\text{prox}}^{\text{eff}}$ [%]	(43)	–	Endoleak type I, SG migration
	Min. stent expansion	[39,18][d]	$e_{\text{min}}^{\text{S}}$ [%]	(24)	↓	SG fatigue, SG kinking
	Max. stent assymetry	[9,11,18][d]	$y_{\text{max}}^{\text{S}}$ [-]	(27)	↓	
	Max. conical stent shape	[92,53][c,d]	$c_{\text{max}}^{\text{S}}$ [-]	(29)	↓	
Pulsatile parameters	Max. graft movement[a]	-	$u_{\text{max}}^{\text{G,pul}}$ [mm]	(31)	↓	SG fatigue
	Max. stent movement[a]		$u_{\text{max}}^{\text{S,pul}}$ [mm]	(32)	↓	
	Mean diametric graft compliance	40,36,61,94,23	$\bar{C}$ [%/100mmHg]	(34)	–	Aortic compliance missmatch

[a]newly introduced EVAR quality parameter; no other publications about this or a closely related parameter is available (to the best of the authors knowledge)

[b] expected or reported influence of the parameter on the quality of EVAR; ↑: high value has positive influence on quality of EVAR; ↓: high value has negative influence on quality of EVAR; –: no unambiguous influence reported

[c] only qualitative assessment/discussion of the EVAR quality parameters but no quantitative considerations of the parameters

[d] consideration of closely related parameters

- Ability to provide indications of potential EVAR related complications
- Quantifiable from in silico EVAR outcomes
- Applicability to patient-specific cases

The following EVAR related complications are considered in this study:

- Endoleak type I[28,12,81,76]
- SG migration[71,95]
- Aortic neck dilatation[17,89,62,21,77,41]
- SG fatigue[35,6]
- SG kinking[14,52]
- Aortic compliance missmatch[83,36,61,87,23]

The in silico EVAR results, i.e. the deployed state of SG and vessel, are postprocessed according to the EVAR quality parameters $q \in \mathcal{Q}$. We focus on scalar-valued parameters to guarantee simple quantitative and statistical investigations. The EVAR quality parameters $q \in \mathcal{Q}$ assess the complication likelihood and hence estimate the potential success of the EVAR outcome. EVAR is considered to be successful if the patient is free of EVAR related complications for several years after the intervention. Nevertheless, all EVAR quality parameters $q \in \mathcal{Q}$ are quantities measured directly after the in silico SG deployment, i.e. they are postinterventional quantities. No growth and remodeling of the aortic tissue is considered which could be used to trace the change of the EVAR quality parameters over time. It is assumed that the EVAR quality parameters as postinterventional quantities already can give hints on potential complications that will occur after several years.

In total, we define 20 EVAR quality parameters. We distinguish between *vessel and stent-graft stresses and tractions* (Section 2.4.1), *fixation and drag forces* (Section 2.4.2), parameters to evaluate the *quality of seal* (Section 2.4.3), *geometrical parameters of the deployed SG* (Section 2.4.4) and *parameters depending on the pulsatile blood pressure* (Section 2.4.5).

In Table 1, all 20 EVAR quality parameters $q \in \mathcal{Q}$ are summarized, their potential impact on the quality of the EVAR outcome is indicated and their related complications are named. In practice, single EVAR complications cannot clearly be separated, of course. For instance, SG migration goes mostly hand in hand with a type I endoleak. However, in Table 1 the intention is to state the relation of the EVAR quality parameter to the EVAR complication it has initiated.

The length of the proximal and distal landing zones of the parameterized vessel and SG of Section 2.2 and 2.3 in the preinterventional configuration are given by (Figure 1)

$$L_{\text{prox}} = \int_{\text{E}_\text{p}}^{\text{S}_\text{p}} \mathrm{d}\hat{s} \approx l_\text{p}, \quad L_{\text{dist}} = \int_{\text{S}_\text{d}}^{\text{E}_\text{d}} \mathrm{d}\hat{s} \approx l_\text{d}. \tag{9}$$

Further, the area of the proximal and distal landing zones of the SG in the preinterventional configuration are given by

$$A_{\text{prox}} = \pi D^{\text{SG}} L_{\text{prox}}, \quad A_{\text{dist}} = \pi D^{\text{SG}} L_{\text{dist}} \tag{10}$$

The area of the proximal landing zone of the SG in the current configuration Ω^{SG}, i.e. in the deployed state, can be calculated by Nanson's formula:

$$a_{\text{prox}} = \int_{\gamma^{\text{G}}_{\text{ex,prox}}} ||\boldsymbol{n}^{\text{G}}|| \mathrm{d}a_{\text{prox}} = \int_{\Gamma^{\text{G}}_{\text{ex,prox}}} ||J^{\text{G}}(\boldsymbol{F}^{\text{G}})^{-\text{T}} \boldsymbol{N}^{\text{G}}|| \mathrm{d}A_{\text{prox}}, \tag{11}$$

where $\boldsymbol{n}^{\text{G}}$ is the unit outward surface normal on the differential area element $\mathrm{d}a_{\text{prox}}$ of the outer graft surface in the current configuration, $\boldsymbol{N}^{\text{G}}$ is the unit outward surface normal on the differential area element $\mathrm{d}A_{\text{prox}}$ of the outer graft surface in the reference configuration, $\boldsymbol{F}^{\text{G}}$ is the deformation gradient and $J^{\text{G}} = \det(\boldsymbol{F}^{\text{G}})$ is the determinant of the deformation gradient. $\gamma^{\text{G}}_{\text{ex,prox}}$ and $\Gamma^{\text{G}}_{\text{ex,prox}}$ are the outer graft surfaces of the proximal landing zone in the current and in the reference configuration, respectively (Figure 1). Same holds for the area of the distal landing zone of the SG in the current configuration

$$a_{\text{dist}} = \int_{\Gamma^{\text{G}}_{\text{ex,dist}}} ||J^{\text{G}}(\boldsymbol{F}^{\text{G}})^{-\text{T}} \boldsymbol{N}^{\text{G}}|| \mathrm{d}A_{\text{dist}}, \tag{12}$$

where the subscript $(\bullet)_{\text{dist}}$ indicates the distal landing zone.

2.4.1 | Vessel and stent-graft stresses and tractions

We apply the Cauchy von Mises equivalent stress measure denoted by σ which is frequently used to asses the stress state in vessels[49,40,70] and SGs[40,54], where σ describes the stress state after the SG deployment. Instead of considering maximum values of stresses, we use stress percentiles which had been proven to be more suitable in the evaluation of vessel stresses[84,49,50]. Accordingly, $\sigma^{\text{wall}}_{99}$ denotes the 99-percentile Cauchy von Mises vessel wall stress which is the stress such that in 99% of the

domain Ω_0^{wall} the Cauchy von Mises stress is smaller than $\sigma_{99}^{\text{wall}}$. A precise mathematical definition of the proposed quantiles is given in Appendix A3.

Aortic neck dilatation is a severe problem after EVAR which is a associated with an enlargement of the vessel in the proximal landing zone and subsequent SG migration or endoleak type Ia. Among other reasons, the additional vessel stress induced by the oversized SG is often named as source of aortic neck dilatation [17,62]. Hence, we introduce the vessel wall overstress $\bar{\sigma}^{\text{wall}}$ by

$$\bar{\sigma}^{\text{wall}}(\boldsymbol{X}) = \sigma(\boldsymbol{X}) - \sigma_{\text{pre}}(\boldsymbol{X}), \quad \forall \boldsymbol{X} \in \Omega_0^{\text{wall}} \tag{13}$$

to measure the additional vessel stress induced by the oversized SG, where $\sigma_{\text{pre}}(\boldsymbol{X})$ are the von Mises Cauchy stresses before EVAR and $\sigma(\boldsymbol{X})$ are the von Mises Cauchy stresses after EVAR (Figure 2I). Here, $\sigma_{\text{pre}}(\boldsymbol{X})$ and $\sigma(\boldsymbol{X})$ both are Cauchy stress measures of the current configuration evaluated at the same material point $\boldsymbol{X} \in \Omega_0^{\text{wall}}$. Accordingly, $\bar{\sigma}_{99}^{\text{wall}}$ is the 99-percentile vessel wall overstress.

A second possible explanation of aortic neck dilatation is the continuation of the aneurysm disease process [21,79]. Actually the SG should protect the diseased vessel by removing the pulsatile blood pressure from the vessel and stopping the disease process. However, if the SG fixation zone is in a partly diseased region, i.e. in a region with partly "aneurysmatic" vessel material, the diseased vessel might not be properly protected. On the contrary, the additional vessel stress induced by the oversized SG might even increase the progression of the disease process in this region since besides biochemical processes vessel stress is considered as one of the triggers of aneurysm growth [8,96]. Hence, we explicitly measure the aneurysmatic vessel wall overstress $\bar{\sigma}^{\lambda,\text{wall}}$ by

$$\bar{\sigma}^{\lambda,\text{wall}}(\boldsymbol{X}) = \lambda(d(\boldsymbol{X}))\left(\sigma(\boldsymbol{X}) - \sigma_{\text{pre}}(\boldsymbol{X})\right) = \lambda(d(\boldsymbol{X}))\,\bar{\sigma}^{\text{wall}}(\boldsymbol{X}), \quad \forall \boldsymbol{X} \in \Omega_0^{\text{wall}}, \tag{14}$$

where $\lambda(d(\boldsymbol{X})) \in [0;1]$ is the blend parameter to distinguish between "healthy" ($\lambda = 0$) and "aneurysmatic" ($\lambda = 1$) vessel material as defined in equation (1). Accordingly, $\bar{\sigma}_{99}^{\lambda,\text{wall}}$ denotes the 99-percentile aneurysmatic vessel wall overstress and describes the maximum additional stress in the "aneurysmatic" vessel wall material compared to the preinterventional vessel wall stresses. Major goal of EVAR is the reduction of vessel wall stresses in the aneurysm sac. Hence, we also quantify the maximum relief $|\bar{\sigma}_1^{\lambda,\text{wall}}|$ of the stresses in the "aneurysmatic" vessel wall material where $\bar{\sigma}_1^{\lambda,\text{wall}}$ denotes the 1-percentile aneurysmatic vessel wall overstress. We clearly want to point out that the definition of the "aneurysmatic" region by $\lambda(d(\boldsymbol{X}))$ is purely heuristic according to the preinterventional local vessel diameter $d(\boldsymbol{X})$. Hence, the stress measure $\bar{\sigma}^{\lambda,\text{wall}}(\boldsymbol{X})$ is affected by this heuristic decision that vessel wall material with an abnormal large vessel diameter is considered to be in an "aneurysmatic" state.

The 99-percentile stent stresses σ_{99}^{S} of the stent in the deployed state are considered to estimate the tendency of SG fatigue. The permanent interaction of vessel and SG with high contact pressures might induce local remodeling of the surrounding tissue or even might lead to erosion of the vessel wall often associated with the emergence of aortoenteric fistula [51,29]. Hence, the magnitude of the normal contact traction

$$t_{\text{n}}(\boldsymbol{x}) = ||\boldsymbol{t}_{\text{n}}(\boldsymbol{x})||, \quad \forall \boldsymbol{x} \in \gamma_{\text{ex}}^{\text{G}} \tag{15}$$

between SG and vessel after the deployment and its 99-percentile value $t_{\text{n},99}$ are considered in this study. In (15), $\boldsymbol{t}_{\text{n}}$ are the normal contact tractions between SG and vessel and $\gamma_{\text{ex}}^{\text{G}}$ is the outer graft surface in the current configuration.

Although the 99-percentile and 1-percentile are used for stresses and tractions in this study, we will speak of maximum and minimum stresses and tractions in the following for simplicity.

2.4.2 | Drag and fixation forces

In the deployed state of the SG, the SG has to sustain the permanent and pulsatile load of the blood flow and pressure. We neglect inertial effects and shear tractions acting on the luminal graft surface since their contribution to the SG drag force is assumed to be negligibly small compared to the hydrostatic blood pressure [34,46,47,44,36]. Hence, we approximate the SG drag force by

$$\boldsymbol{F}_{\text{drag}} = \int_{\gamma_{\text{l}}^{\text{G}}} \hat{\boldsymbol{t}}^{\text{G}}\, \text{d}a_{\text{l}}^{\text{G}} \approx -p \int_{\gamma_{\text{l}}^{\text{G}}} \boldsymbol{n}^{\text{G}}\, \text{d}a_{\text{l}}^{\text{G}} \tag{16}$$

where $\hat{\boldsymbol{t}}^{\text{G}}$ is the nonlinear traction load of the blood on the luminal graft surface $\gamma_{\text{l}}^{\text{G}}$. $\boldsymbol{n}^{\text{G}}$ is the unit outward surface normal on the differential area element $\text{d}a_{\text{l}}^{\text{G}}$ of the luminal graft surface in the current configuration and p is the hydrostatic blood pressure.

In order to resist the SG drag force $\boldsymbol{F}_{\text{drag}}$ and prevent the SG from migrating, SGs generally are designed with an oversize with respect to the vessel diameter (equation (5)). The SG oversizing results in a passive fixation force

$$\hat{F}_{\text{prox}} = \int_{\gamma^{\text{G}}_{\text{ex,prox}}} ||\boldsymbol{t}_{\text{n}}||\, \text{d}a_{\text{prox}}, \quad \hat{F}_{\text{dist}} = \int_{\gamma^{\text{G}}_{\text{ex,dist}}} ||\boldsymbol{t}_{\text{n}}||\, \text{d}a_{\text{dist}} \tag{17}$$

in the proximal and in the distal landing zone, respectively (Figure 2II). In (17), $\boldsymbol{t}_{\text{n}}$ is the normal contact traction at the contact interface between SG and luminal surface of the vessel.

2.4.3 | Quality of seal

To obtain an optimal seal between SG and vessel in the proximal and distal landing zone, the fixation areas in the landing zones of the SG should be as large as possible. Here, we exemplarily consider the fixation area in the proximal landing zone, also denoted as endograft apposition surface [80], which is given by

$$a^{\text{seal}}_{\text{prox}} = \int_{\gamma^{\text{G}}_{\text{ex,prox}}} (1 - \text{sgn}(g_{\text{n}}))\text{d}a_{\text{prox}}. \tag{18}$$

In (18), g_{n} is the gap function between the potential contact surfaces in the current configuration and sgn(•) is the sign function. According to the Karush-Kuhn-Tucker conditions of unilateral contact [69], the gap function is $g_{\text{n}} \geq 0$ and consequently for points being in contact, sgn(g_{n}) is zero and for points not being in contact sgn(g_{n}) is one. In contrast to the area a_{prox} of the proximal landing zone (equation (11)), the fixation area $a^{\text{seal}}_{\text{prox}}$ is only the portion of a_{prox} that is in contact with the vessel (Figure 2III). From a mechanical perspective, $a^{\text{seal}}_{\text{prox}}$ should be as large as possible, such that SG fixation forces are distributed over a larger area and hence the fixation is more uniform and stable against SG migration.

Type I endoleaks occur when a gap between SG and vessel in the landing zones allows blood to flow into the aneurysm sac. Hence, to further assess the quality of seal, we determine the closest point distance s^{GA} of each point $\boldsymbol{x}^{\text{G}} \in \Omega^{\text{G}}_{\text{prox}}$ of the graft as well as the closest point distance s^{SA} of each point $\boldsymbol{x}^{\text{S}} \in \Omega^{\text{S}}_{\text{prox}}$ of the stent on the luminal vessel surface with $\boldsymbol{x}^{\text{Ao}} \in \gamma^{\text{Ao}}_{\text{l}}$ and evaluate their maximum values by

$$s^{\text{GA}}_{\text{max}} = \max_{\boldsymbol{x}^{\text{G}} \in \Omega^{\text{G}}_{\text{prox}}} s^{\text{GA}}(\boldsymbol{x}^{\text{G}}) = \max_{\boldsymbol{x}^{\text{G}} \in \Omega^{\text{G}}_{\text{prox}}} \left(\boldsymbol{n}^{\text{Ao}}(\check{\boldsymbol{x}}^{\text{Ao,G}}) \cdot (\boldsymbol{x}^{\text{G}} - \check{\boldsymbol{x}}^{\text{Ao,G}}) \right) \tag{19}$$

and

$$s^{\text{SA}}_{\text{max}} = \max_{\boldsymbol{x}^{\text{S}} \in \Omega^{\text{S}}_{\text{prox}}} s^{\text{SA}}(\boldsymbol{x}^{\text{S}}) = \max_{\boldsymbol{x}^{\text{S}} \in \Omega^{\text{S}}_{\text{prox}}} \left(\boldsymbol{n}^{\text{Ao}}(\check{\boldsymbol{x}}^{\text{Ao,S}}) \cdot (\boldsymbol{x}^{\text{S}} - \check{\boldsymbol{x}}^{\text{Ao,S}}) \right), \tag{20}$$

respectively. $\Omega^{\text{G}}_{\text{prox}}$ and $\Omega^{\text{S}}_{\text{prox}}$ are the current configurations of the proximal landing zone of the graft and the stent, respectively (Figure 1). $\boldsymbol{n}^{\text{Ao}}$ is the outward surface normal on $\gamma^{\text{Ao}}_{\text{l}}$ in the current configuration (Figure 2III, detail Z). In (19), $\check{\boldsymbol{x}}^{\text{Ao,G}}(\boldsymbol{x}^{\text{G}})$ is the point on the luminal vessel surface $\gamma^{\text{Ao}}_{\text{l}}$ that is closest to the point $\boldsymbol{x}^{\text{G}} \in \Omega^{\text{G}}$, i.e.

$$\check{\boldsymbol{x}}^{\text{Ao,G}}(\boldsymbol{x}^{\text{G}}) = \underset{\boldsymbol{x}^{\text{Ao}} \in \gamma^{\text{Ao}}_{\text{l}}}{\text{argmin}} ||\boldsymbol{x}^{\text{G}} - \boldsymbol{x}^{\text{Ao}}||. \tag{21}$$

Analogously, in (20) $\check{\boldsymbol{x}}^{\text{Ao,S}}(\boldsymbol{x}^{\text{S}})$ is determined by

$$\check{\boldsymbol{x}}^{\text{Ao,S}}(\boldsymbol{x}^{\text{S}}) = \underset{\boldsymbol{x}^{\text{Ao}} \in \gamma^{\text{Ao}}_{\text{l}}}{\text{argmin}} ||\boldsymbol{x}^{\text{S}} - \boldsymbol{x}^{\text{Ao}}||. \tag{22}$$

In the following, we denote $s^{\text{SA}}_{\text{max}}$ and $s^{\text{GA}}_{\text{max}}$ as the maximum stent-vessel gap and the maximum graft-vessel gap, respectively.

2.4.4 | Geometrical parameters of the deployed stent-graft

Given the centerline C_{De} of the SG in the deployed state which is parametrized by its arc length $s_{\text{De}} \in [0; L^{\text{SG}}_{\text{De}}]$, in slices $\gamma^{\text{SG}}_{\perp}(s_{\text{De}})$ orthogonal to the centerline C_{De}, the average radius $\bar{r}^{\text{S}}(s_{\text{De}})$, the minimal radius $r^{\text{S}}_{\text{min}}(s_{\text{De}})$ and the maximum radius $r^{\text{S}}_{\text{max}}(s_{\text{De}})$ of the stent are evaluated (Figure 2IV). The calculation of the centerline C_{De} of the SG in the deployed state is not discussed in this contribution. The interested reader can find detailed information on this topic in [33]. We only evaluate the geometrical shape of the stent since the geometrical shape of the graft is dominated by its buckling pattern and does not represent the effects that shall be investigated in this section.

The degree of stent expansion (Figure 2IV) is defined by

$$e^{\mathrm{S}}(s_{\mathrm{De}}) = \frac{\bar{d}^{\mathrm{S}}(s_{\mathrm{De}})}{D^{\mathrm{SG}}} = \frac{2\bar{r}^{\mathrm{S}}(s_{\mathrm{De}})}{D^{\mathrm{SG}}}, \quad \forall s_{\mathrm{De}} \in [0; L_{\mathrm{De}}^{\mathrm{SG}}], \tag{23}$$

where D^{SG} is the nominal diameter of the SG and $\bar{d}^{\mathrm{S}}(s_{\mathrm{De}})$ is the average diameter of the stent in the slice $\gamma_{\perp}^{\mathrm{SG}}(s_{\mathrm{De}})$. The minimum stent expansion

$$e_{\mathrm{min}}^{\mathrm{S}} = \min_{s_{\mathrm{De}} \in [0; L_{\mathrm{De}}^{\mathrm{SG}}]} e^{\mathrm{S}}(s_{\mathrm{De}}), \tag{24}$$

expresses the degree of compression of the stent rings and hence might have an influence on the fatigue behavior of the SG. Minimum values $e_{\mathrm{min}}^{\mathrm{S}}$ of the stent expansion are primarily be found in the landing zones where the full expansion of the stent is restricted by the surrounding vessel.

Furthermore, the effective degree of SG oversizing at a specific location s_{De} can be calculated by

$$o_{\mathrm{eff}}(s_{\mathrm{De}}) = \frac{D^{\mathrm{SG}}}{\bar{d}^{\mathrm{S}}(s_{\mathrm{De}})} - 1 = \frac{1}{e^{\mathrm{S}}(s_{\mathrm{De}})} - 1, \quad \forall s_{\mathrm{De}} \in [0; L_{\mathrm{De}}^{\mathrm{SG}}]. \tag{25}$$

In contrast to the nominal degree of SG oversizing o (equation 5), the effective degree of SG oversizing o_{eff} expresses the degree of SG oversizing in the deployed state of the SG. Since the vessel is elastically deformable, the insertion of a SG generally leads to an enlargement of the vessel diameter in the landing zones. Hence, if the SG is perfectly aligned to the luminal vessel surface the effective degree of SG oversizing o_{eff} is generally smaller than the nominal value of SG oversizing o in an elastically deformable vessel. For a rigid vessel, nominal and effective degree of SG oversizing would be identical in this case. The mean value of the effective degree of SG oversizing in the proximal landing zone is denoted by

$$\bar{o}_{\mathrm{prox}}^{\mathrm{eff}} = \frac{1}{L_{\mathrm{prox}}} \int_0^{L_{\mathrm{prox}}} o_{\mathrm{eff}}(s_{\mathrm{De}}) \mathrm{d}s_{\mathrm{De}}, \tag{26}$$

The best seal between SG and vessel and the most uniform fixation of the SG in cylindrically shaped landing zones can be assumed for a perfectly cylindrical shape of the SG in the deployed state. Any asymmetric shape of the SG in the deployed state might have negative effects on the seal and the fixation[92,9] but also on the fatigue behavior of the SG since asymmetric stent shapes go hand in hand with nonuniform loading of the SG with local stress hot spots. The stent asymmetry y^{S} and its maximum value are defined by

$$y_{\mathrm{max}}^{\mathrm{S}} = \max_{s_{\mathrm{De}} \in [0; L_{\mathrm{De}}^{\mathrm{SG}}]} y^{\mathrm{S}}(s_{\mathrm{De}}) = \max_{s_{\mathrm{De}} \in [0; L_{\mathrm{De}}^{\mathrm{SG}}]} \left(\frac{r_{\mathrm{max}}^{\mathrm{S}}(s_{\mathrm{De}})}{r_{\mathrm{min}}^{\mathrm{S}}(s_{\mathrm{De}})} - 1 \right). \tag{27}$$

This means that $y^{\mathrm{S}}(s_{\mathrm{De}})$ is a measure of the ovalization of the stent which is 0 in the case of a perfectly circular shape and $y^{\mathrm{S}}(s_{\mathrm{De}}) > 0$ for any elliptic shape of the stent (Figure 2IV).

If the SG is forced in a conical shape, this can also lead to negative effects on the fixation and the fatigue behavior of the SG[53,92]. The conical shape of a stent limb $i \in [1; n^{\mathrm{S}}]$ is defined as

$$c_i^{\mathrm{S}} = \frac{\max\limits_{s_{\mathrm{De}} \in \mathrm{S}_i} \bar{r}^{\mathrm{S}}(s_{\mathrm{De}})}{\min\limits_{s_{\mathrm{De}} \in \mathrm{S}_i} \bar{r}^{\mathrm{S}}(s_{\mathrm{De}})} - 1, \tag{28}$$

where n^{S} is the number of stent limbs of the SG and S_i is the interval of the arc length s_{De} of the centerline C_{De} that corresponds to the position of stent limb i. For a perfectly cylindrical stent limb $c_i^{\mathrm{S}} = 0$ and for a stent limb of conical shape $c_i^{\mathrm{S}} > 0$ (Figure 2IV). The stent limb with the maximum conical shape is denoted as

$$c_{\mathrm{max}}^{\mathrm{S}} = \max_{i \in [1; n^{\mathrm{S}}]} c_i^{\mathrm{S}} \tag{29}$$

Furthermore, strongly asymmetric and conical stent shapes might be an indicator of local SG kinking.

2.4.5 | Parameters depending on the pulsatile blood pressure

The SG is subjected to the permanent pulsatile nature of blood flow with the relative displacement

$$\boldsymbol{u}^{\mathrm{pul}}(\boldsymbol{X}) = \boldsymbol{u}^{\mathrm{sys}}(\boldsymbol{X}) - \boldsymbol{u}^{\mathrm{diast}}(\boldsymbol{X}), \quad \forall \boldsymbol{X} \in \Omega_0^{\mathrm{SG}}. \tag{30}$$

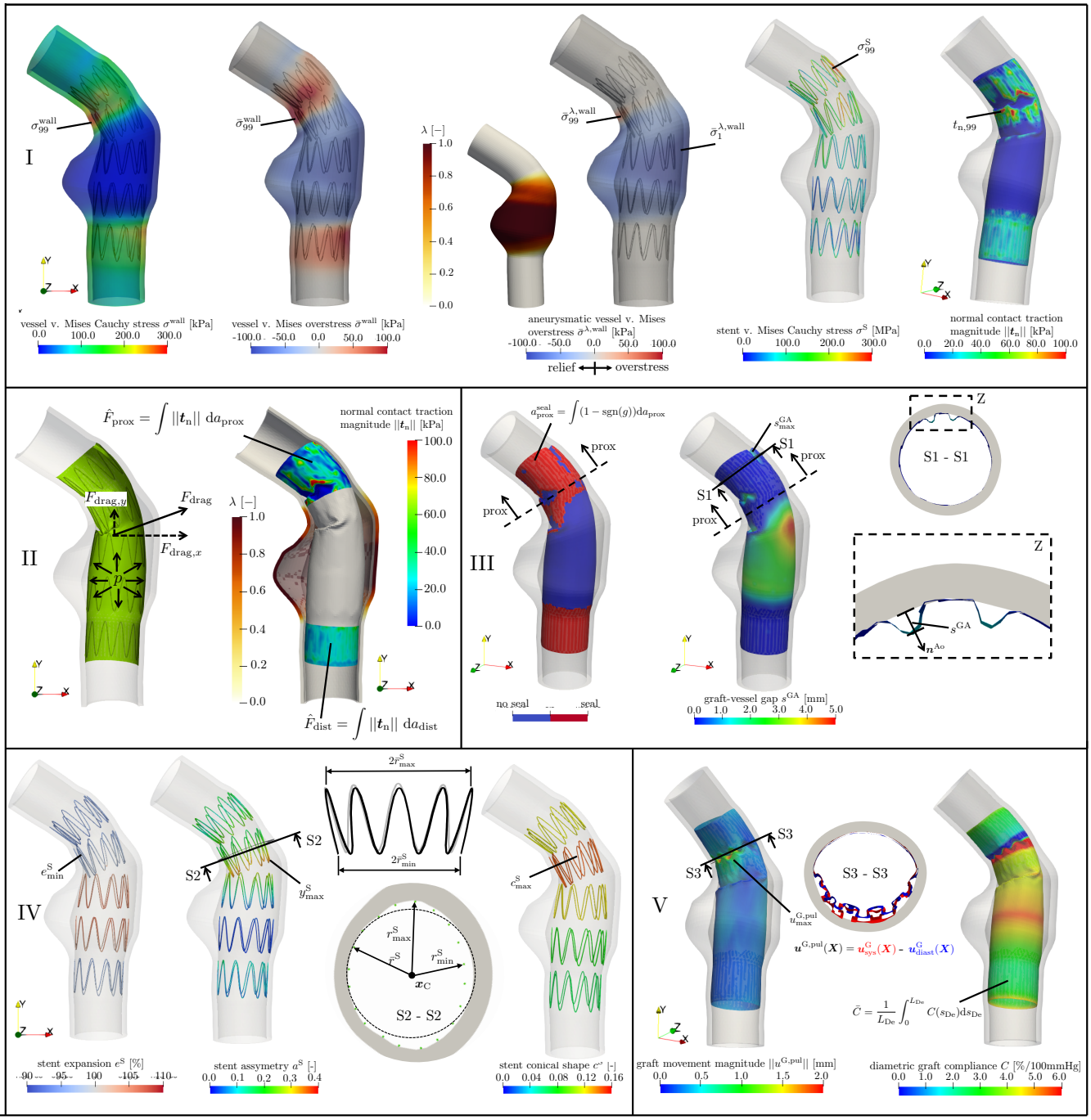

FIGURE 2 Qualitative visualization of the EVAR quality parameters $q \in \mathcal{Q}$: Vessel and stent-graft stresses and tractions (I), fixation and drag forces (II), quality of seal (III), geometrical parameters of the deployed SG (IV) and parameters depending on the pulsatile blood pressure (V).

where $\boldsymbol{u}^{\text{sys}}(\boldsymbol{X})$ is the displacement of material point $\boldsymbol{X}$ at the systolic pressure state and $\boldsymbol{u}^{\text{diast}}(\boldsymbol{X})$ is the displacement of the same material point $\boldsymbol{X}$ at the diastolic pressure state.

We quantitatively determine the maximal movement of the stent $u^{\text{S,pul}}_{\text{max}}$ and the graft $u^{\text{G,pul}}_{\text{max}}$ during one heart beat by

$$u^{\text{G,pul}}_{\text{max}} = \max_{\boldsymbol{X} \in \Omega^{\text{G}}_0} ||\boldsymbol{u}^{\text{pul}}(\boldsymbol{X})|| \tag{31}$$

and

$$u_{\max}^{\mathrm{S,pul}} = \max_{\boldsymbol{X}\in\Omega_0^{\mathrm{S}}} ||\boldsymbol{u}^{\mathrm{pul}}(\boldsymbol{X})||, \tag{32}$$

respectively (Figure 2V). Obviously, large permanent movements of a material point $\boldsymbol{X}$ together with high strains and stresses at this point might increase the risk of SG fatigue dramatically.

Arterial compliance is defined as the ratio of change in arterial blood volume to change in arterial blood pressure [36,13]. It is well known that the insertion of a SG reduces the compliance in this region generally denoted as aortic compliance mismatch. This might have negative effects such as increased pressure wave reflection, decreased distal perfusion and increased pulsatile stresses and vessel distension of the vessel at the interface between the native, compliant vessel and the SG with reduced compliance [61,23,82,36]. The latter effect of increased pulsatile vessel stresses and vessel distension is mentioned as main initiator of aortic neck dilatation by some studies [82,23]. Instead of measuring the volume change mostly the change in diameter or the change in cross section is used to determine arterial compliance [90,30,45,94,61,36]. Analogously, we calculate the compliance of the graft in the deployed state by

$$C(s_{\mathrm{De}}) = \frac{\left(\frac{\bar{d}^{\mathrm{sys,G}}(s_{\mathrm{De}})-\bar{d}^{\mathrm{diast,G}}(s_{\mathrm{De}})}{\bar{d}^{\mathrm{diast,G}}(s_{\mathrm{De}})}\right)}{p^{\mathrm{sys}}-p^{\mathrm{diast}}}, \quad \forall s_{\mathrm{De}} \in [0; L_{\mathrm{De}}^{\mathrm{SG}}], \tag{33}$$

where p^{diast} is the diastolic blood pressure, p^{sys} is the systolic blood pressure and $s_{\mathrm{De}} \in [0; L_{\mathrm{De}}^{\mathrm{SG}}]$ is the arc length of the SG centerline in the deployed state. $\bar{d}^{\mathrm{diast,G}}(s_{\mathrm{De}})$ and $\bar{d}^{\mathrm{sys,G}}(s_{\mathrm{De}})$ are the average graft diameters in orthogonal slices $\gamma_{\perp}^{\mathrm{SG}}(s_{\mathrm{De}})$ at the diastolic and the systolic blood pressure state, respectively. We only consider average diameters of the graft $\bar{d}^{\mathrm{diast,G}}(s_{\mathrm{De}})$ and $\bar{d}^{\mathrm{sys,G}}(s_{\mathrm{De}})$ (not the average diameters of the stent) since the domain of the lumen is fully described by the graft. Obviously, in the landing zones the compliance $C(s_{\mathrm{De}})$ is smaller than in the aneurysm sac, since in the landing zones the compliance is a superposition of the compliance of the SG and the surrounding vessel. In the aneurysm sac, where generally there is only partial contact between SG and vessel, the compliance $C(s_{\mathrm{De}})$ is dominated solely by the compliance of the SG. Hence, depending on the position $s_{\mathrm{De}} \in [0; L_{\mathrm{De}}^{\mathrm{SG}}]$, the compliance $C(s_{\mathrm{De}})$ is either a superposition of the compliance of SG and vessel or the compliance of the SG only (Figure 2V). Quantitatively, we only consider the mean diametric compliance $\bar{C}$ given by

$$\bar{C} = \frac{1}{L_{\mathrm{De}}^{\mathrm{SG}}} \int_0^{L_{\mathrm{De}}^{\mathrm{SG}}} C(s_{\mathrm{De}})\mathrm{d}s. \tag{34}$$

2.5 | Framework of the parameter study

Using the 22 geometrical parameters $g \in \mathcal{G} = \mathcal{G}^{\mathrm{Ao}} \cup \mathcal{G}^{\mathrm{SG}}$ and the nominal degree of SG oversizing o, the vessel and the SG are uniquely defined in their preinterventional configuration Ω_0^{Ao} and Ω_0^{SG}, respectively (Figure 1). In the following, variations of vessel parameters $g^{\mathrm{Ao}} \in \mathcal{G}^{\mathrm{Ao}}$ and SG parameters $g^{\mathrm{SG}} \in \mathcal{G}^{\mathrm{SG}}$ around the basic vessel and SG with the parameters $\hat{g}$ (Table 2) are considered and their influence on the EVAR quality parameters $q \in \mathcal{Q}$ is investigated. Since a full factorial analysis for the given number of parameters $g \in \mathcal{G}$ and the number of parameter variations is not achievable, we use a basic vessel and SG geometry from which single parameters $g \in \mathcal{G}$ are modified while all others are kept constant. For each realization of the parameters $g \in \mathcal{G}$, the deployed SG configuration is evaluated at the hydrostatic, diastolic blood pressure level of $p^{\mathrm{diast}} = 80$ mmHg and at the hydrostatic, systolic blood pressure level of $p^{\mathrm{sys}} = 130$ mmHg since some EVAR quality parameters might be critical in the diastolic state, others in the systolic state. We consider 73 different realizations of the parameters $g \in \mathcal{G}$ (Table 2) which together with the two considered blood pressure states results in $n = 73 \cdot 2 = 146$ required simulations. $n^{\mathrm{Ao}} = 120$ and $n^{\mathrm{SG}} = 26$ different realizations of the vessel parameters and the SG parameters are used.

Figure 3 provides an overview of the proposed framework to assess relations between the vessel as well as SG parameters $g \in \mathcal{G}$ and the EVAR quality parameters $q \in \mathcal{Q}$. For each realization of the parameters $g \in \mathcal{G}$ we use the in silico EVAR methodology proposed in [32] to deploy the SG with a nominal degree of oversizing of $o_1 = 5\%$. Subsequently, we investigate the degrees of SG oversizing in the range between $o_1 = 5\%$ to $o_2 = 40\%$ in a computationally efficient way by using SG parameter continuation [32]. Using parameter continuation, it is possible to model all degrees of SG oversizing in the range $o \in [o_1, o_2] = [\frac{D_1^{\mathrm{SG}}}{d_{\mathrm{p}}} - 1, \frac{D_2^{\mathrm{SG}}}{d_{\mathrm{p}}} - 1]$ within one in silico EVAR simulation. Starting from the results of an in silico EVAR simulation, i.e. the deployed state of SG and vessel, with a SG of diameter D_1^{SG} the stress-free reference configuration of the SG is continuously

TABLE 2 Overview of vessel and SG parameters: basic paramters $\hat{g}$ that describe the basic vessel and SG configuration, range $[g_{\min}; g_{\max}]$ and number of variations $\#g_i$ of the parameters used in the parameter study. Parameters highlighted in gray are varied in the parameter study.

	Vessel parameters $g^{\mathrm{Ao}} \in \mathcal{G}^{\mathrm{Ao}}$													
	α_{p}	α_{d}	l_{p}	l_{d}	d [a]	e [b]	l_{AAA}	d_{AAA}	$l_{\mathrm{sp}}^{\mathrm{c,d}}$	l_{sd}	t_{w}	t_{ILT}	γ	$\bar{c}_{\mathrm{prox}}^{\mathrm{Ao}}$ [e]
	[°]	[°]	[mm]	[mm]	[mm]	[mm]	[mm]	[mm]	[mm]	[mm]	[mm]	[mm]	[-]	[%]
$\hat{g}$	50	0	25	15	24	5	60	45	20	20	1.5	10	1	0
$g_{\min}$	-80	0	5	15	16	0	40	45	10	20	0.68	0	0.125	0
$g_{\max}$	80	0	30	15	32	12	100	45	40	20	2.6	28	8	70
$\#g_i$	13	1	6	1	5	6	4	1	8	1	7	6	7	7

	SG parameters $g^{\mathrm{SG}} \in \mathcal{G}^{\mathrm{SG}}$					
	h^{S}	p^{S}	n^{S}	ω	t^{S}	t^{G}
	[mm]	[-]	[-]	[%]	[mm]	[mm]
$\hat{g}$	16	10	5	5	0.33	0.05
$g_{\min}$	8	4	(5)[f]	0	0.33	0.05
$g_{\max}$	28	14	(5)[f]	25	0.33	0.05
$\#g_i$	6	4	(1)[f]	6	1	1

[a] same vessel diameters $d = d_{\mathrm{p}} = d_{\mathrm{d}}$ are used in the proximal and distal neck
[b] same neck eccentricities $e = e_{\mathrm{p}} = e_{\mathrm{d}}$ are used
[c] use of shortened neck length $l_{\mathrm{p}} = 5$ mm to increase potential influence of l_{sp}
[d] 4 variations of l_{sp} at $\alpha_{\mathrm{p}} = 0°$ and 4 variations of l_{sp} at $\alpha_{\mathrm{p}} = 50°$
[e] variation of percentage circumferential proximal neck calcification $\bar{c}_{\mathrm{prox}}^{\mathrm{Ao}}$ and location of the calcification spots
[f] n^{S} adapted to SG length L^{SG} (equ. (4)); gap between stent limbs is kept constant

changed to the larger diameter D_2^{SG} which corresponds to the nominal degree of SG oversizing of o_2 (Figure 3III). The stress-free reference configurations of stent and graft are modified such that the degree of stent predeformation ω remains constant during SG parameter continuation.

Such a study would be computationally extremely expensive if SG parameter continuation is not used since for each considered degree of SG oversize, a separate in silico EVAR simulation would be required. Assuming that the degree of SG oversizing should be investigated in increments of 5% in the range from 5% to 40%, such a study would require eight in silico EVAR simulations per considered parameter realization. Together with the large amount of considered realizations of the parameters $g \in \mathcal{G}$ in this study, this would result in $8 \cdot 146 = 1168$ required in silico EVAR simulations which is not achievable with a reasonable amount of computational power. Further, SG parameter continuation not only provides results of discrete nominal degrees of SG oversizing but provides the results continuously over different nominal degrees of SG oversizing within the provided range $o \in [o_1, o_2]$.

Each deployed SG configuration with $o \in [o_1, o_2]$ is postprocessed according to the EVAR quality parameters $q \in \mathcal{Q}$ to assess the quality of the EVAR outcome with respect to EVAR complication likelihoods (Figure 3IV). Hence, as a result of the proposed parameter study, we obtain the EVAR quality parameters $q(g^{\mathrm{Ao}}, g^{\mathrm{SG}}, o)$ as a function of g^{Ao}, g^{SG} and o where g^{Ao} and g^{SG} are discrete function parameters and o is a continuously given function parameter.

For the purpose of a statistical analysis, we consider the coefficient of variation

$$\mathrm{CV}q(o) = \frac{\sigma_q(o)}{\mu_q(o)}, \quad \forall q \in \mathcal{Q} \tag{35}$$

where

$$\mu_q(o) = \operatorname*{mean}_{i=1,2,\dots,n} q_i(o), \quad \forall q \in \mathcal{Q} \tag{36}$$

is the mean value and

$$\sigma_q(o) = \operatorname*{std}_{i=1,2,\dots,n} q_i(o), \quad \forall q \in \mathcal{Q}, \tag{37}$$

is the the standard deviation. q_i is the value of EVAR quality parameter $q \in \mathcal{Q}$ for the specific realization $i = 1, 2, ..., n$ that is described by the vessel and SG parameters g_i. Coefficients of variation $\mathrm{CV}q(o)$, mean values $\sigma_q(o)$ and standard deviations $\sigma_q(o)$ are continuously given for all considered degrees of SG oversizing $o \in [5\%; 40\%]$ since the EVAR quality parameters $q_i(o)$ are evaluated continuously in this range of SG oversizing.

Further, in order to investigate correlations, the degree of SG oversizing is not considered as continuous but also as discrete design variable. This leads to $\tilde{n} = n \cdot n_o = 146 n_o$ realizations at which the EVAR quality parameters $q \in \mathcal{Q}$ are given by discrete values q_i where n_o is the number of discrete evaluations of the continuously given nominal degree of SG oversizing o.

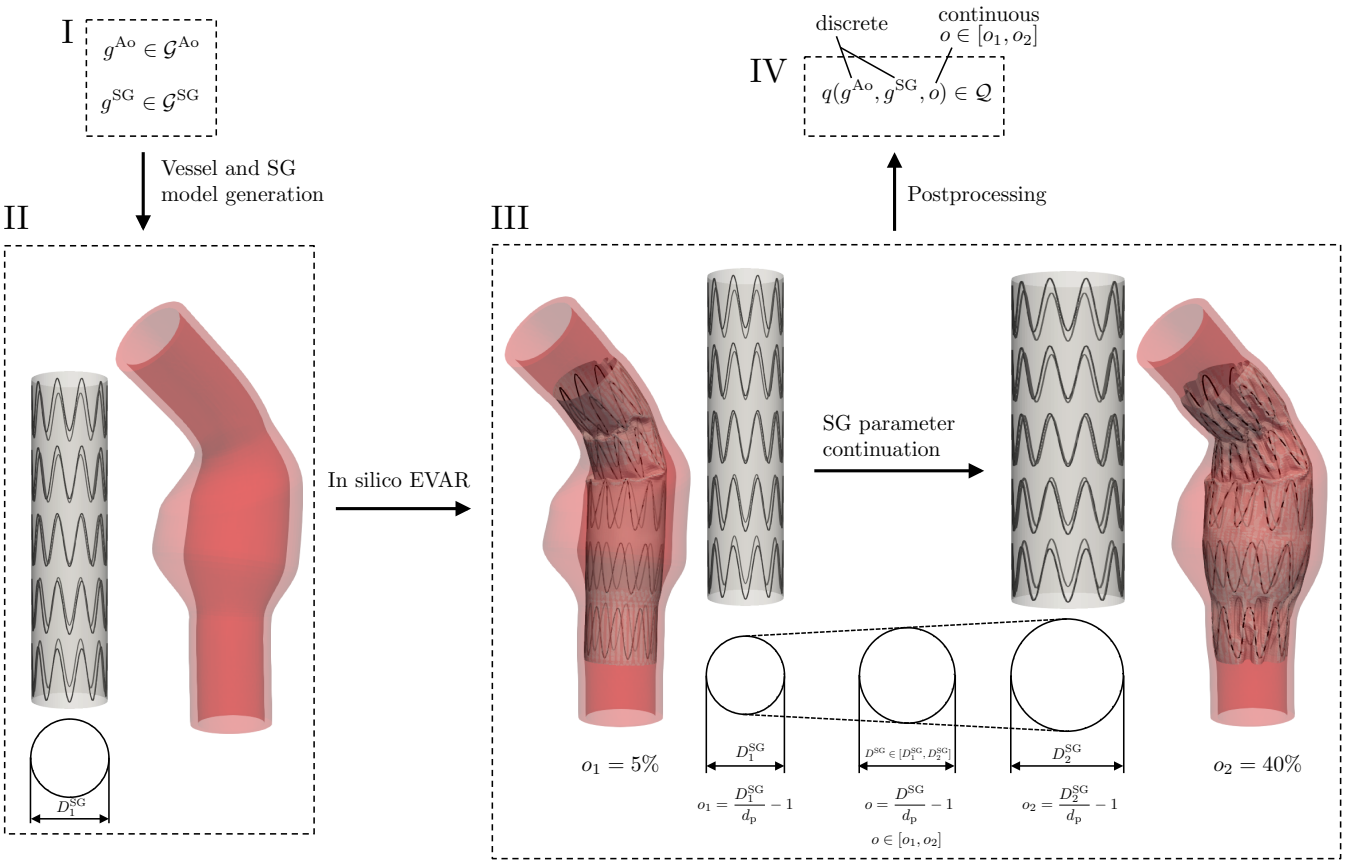

FIGURE 3 Framework of the parameter study: vessel and SG parameter selection (I), vessel and SG model generation with an initial degree of SG oversizing of $o_1 = 5\%$ (II), parameter continuation to continuously change the degree of SG oversizing from $o_1 = 5\%$ to $o_2 = 40\%$ without having to perform an in silico SG deployment again (III), evaluation of the EVAR quality parameters $q \in \mathcal{Q}$ for the deployed SG configurations of all SGs with $o \in [o_1; o_2]$ (IV).

The Pearson product-moment correlation coefficient between the EVAR quality parameter $q \in \mathcal{Q}$ and the nominal degree of SG oversizing o is given by

$$r_{q,o} = \frac{\sum_{i=1}^{\tilde{n}} (q_i - \bar{q})(o_i - \bar{o})}{\sqrt{\sum_{i=1}^{\tilde{n}} (q_i - \bar{q})^2} \sqrt{\sum_{i=1}^{\tilde{n}} (o_i - \bar{o})^2}}, \quad \forall q \in \mathcal{Q},\ o \in [o_1, o_2], \tag{38}$$

where $\bar{q}$ and $\bar{o} = 22.5\%$ are the mean values over all $\tilde{n}$ realizations of the EVAR quality parameter $q \in \mathcal{Q}$ and the degree of SG oversizing o, respectively. The correlation between two EVAR quality parameters $\hat{q} \in \mathcal{Q}$ and $\check{q} \in \mathcal{Q}$ is given by

$$r_{\hat{q},\check{q}} = \frac{\sum_{i=1}^{\tilde{n}} (\hat{q}_i - \bar{\hat{q}})(\check{q}_i - \bar{\check{q}})}{\sqrt{\sum_{i=1}^{\tilde{n}} (\hat{q}_i - \bar{\hat{q}})^2} \sqrt{\sum_{i=1}^{\tilde{n}} (\check{q}_i - \bar{\check{q}})^2}}, \quad \forall \hat{q}, \check{q} \in \mathcal{Q} \tag{39}$$

where $\bar{\hat{q}}$ and $\bar{\check{q}}$ are the mean values of the EVAR quality parameter $\hat{q} \in \mathcal{Q}$ and the EVAR quality parameter $\check{q} \in \mathcal{Q}$, respectively.

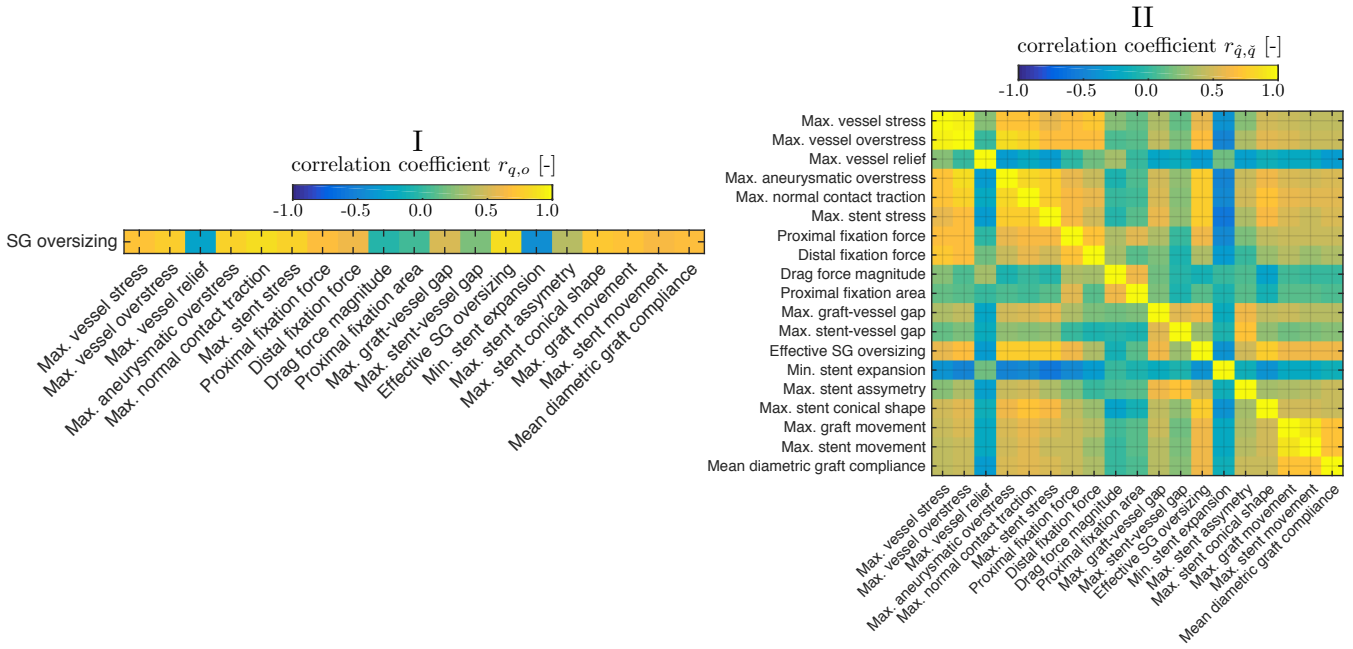

FIGURE 4 Correlation coefficients $r_{q,o}$ between EVAR quality parameters $q \in Q$ and the degree of SG oversizing o (I) and correlation coefficients $r_{\hat{q},\check{q}}$ between EVAR quality parameters $\hat{q}$ and $\check{q}$ (II) as defined in equation (38) and equation (39), respectively.

3 | RESULTS

Due to the large amount of data, we only show the most interesting findings in this section. The interested reader is referred to Appendix A4 for a more detailed summary of the simulation results. This section is organized as follows: first, statistical studies on the total cohort of $n = 146$ realizations are performed with respect to the influence of vessel and SG parameters as well as the degree of SG oversizing on the EVAR quality parameters (Section 3.1). Afterwards more specific quantitative and qualitative results are presented for variations of the degree of SG oversizing (Section 3.2), variations of the vessel (Section 3.3), variations of the SG (Section 3.4) and variations of the arterial blood pressure state (Section 3.5). Finally, the presented methods are applied to four patient-specific cases (Section 3.6).

3.1 | Correlation results and the overall impact of vessel and stent-graft parameters

Strong positive correlation with correlation coefficients $r_{q,o} > 0.75$ is given between the degree of SG oversizing o and the following EVAR quality parameters (Figure 4I): maximum vessel overstress $\bar{\sigma}_{99}^{\text{wall}}$, maximum aneurysmatic overstress $\bar{\sigma}_{99}^{\lambda,\text{wall}}$, maximum normal contact traction $t_{\text{n},99}$, maximal stent stress σ_{99}^{S} and the effective degree of SG oversizing $\bar{o}_{\text{prox}}^{\text{eff}}$. No correlation is given between the nominal degree of SG oversizing o and the SG drag force $\boldsymbol{F}_{\text{drag}}$ ($r_{q,o} = -0.05$) as well as between the nominal degree of SG oversizing o and the proximal fixation area $a_{\text{prox}}^{\text{seal}}$ ($r_{q,o} = 0.04$). The last point indicates that a larger area A_{prox} that results from a larger SG diameter D^{SG} (equation (10)) does not necessarily lead to a larger proximal fixation area $a_{\text{prox}}^{\text{seal}}$ since buckling of the graft reduces the graft-vessel attachment in case of larger degrees of SG oversizing o.

Figure 4II shows the correlation between the single EVAR quality parameters $q \in Q$. Strong correlation between maximum aneurysmatic overstress $\bar{\sigma}_{99}^{\lambda,\text{wall}}$ and the maximum normal contact traction $t_{\text{n},99}$ ($r_{\hat{q},\check{q}} = 0.81$), between the maximum aneurysmatic overstress $\bar{\sigma}_{99}^{\lambda,\text{wall}}$ and the maximum stent stresses σ_{99}^{S} ($r_{\hat{q},\check{q}} = 0.76$) as well as between the normal contact traction $t_{\text{n},99}$ and the maximum stent stresses σ_{99}^{S} ($r_{\hat{q},\check{q}} = 0.75$) is given. Further, the effective degree of SG oversizing $\bar{o}_{\text{prox}}^{\text{eff}}$ strongly correlates with the maximum aneurysmatic overstress $\bar{\sigma}_{99}^{\lambda,\text{wall}}$ ($r_{\hat{q},\check{q}} = 0.76$), the maximum normal contact traction $t_{\text{n},99}$ ($r_{\hat{q},\check{q}} = 0.78$) and the maximum stent stresses σ_{99}^{S} ($r_{\hat{q},\check{q}} = 0.75$). Strong, but less surprising correlations are given between the maximum vessel stress $\sigma_{99}^{\text{wall}}$ and the maximum vessel overstress $\bar{\sigma}_{99}^{\text{wall}}$ ($r_{\hat{q},\check{q}} = 0.94$), the maximum vessel overstress $\bar{\sigma_{99}}^{\text{wall}}$ and the maximum

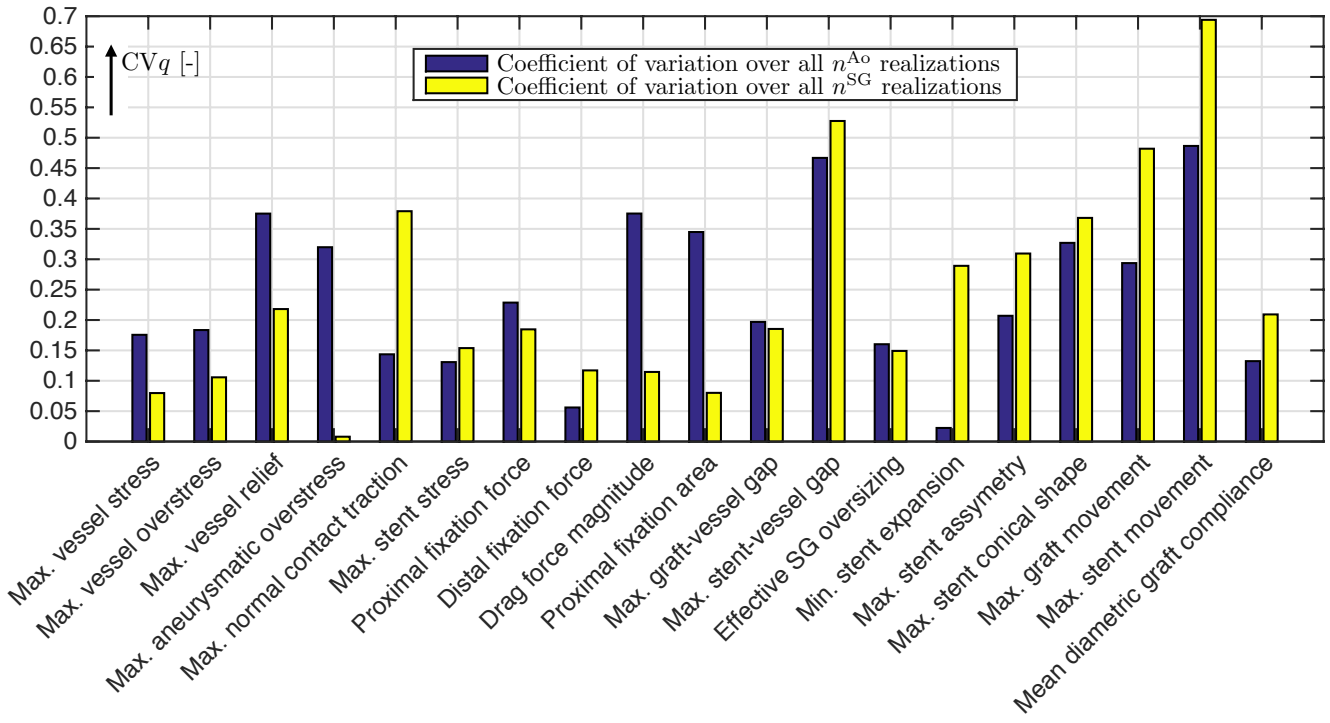

FIGURE 5 Coefficient of variation CVq (equation (35)) over all $n^{\mathrm{Ao,diast}}$ realizations with different vessel geometries (blue bars) as well as over all $n^{\mathrm{SG,diast}}$ realizations with different SG geometries (yellow bars) for a nominal degree of SG oversizing of $o = 15\%$ at the diastolic pressure level of $p^{\mathrm{diast}} = 80$ mmHg.

aneurysmatic overstress $\bar{\sigma}_{99}^{\lambda,\mathrm{wall}}$ ($r_{\hat{q},\check{q}} = 0.85$) as well as between the maximum graft movement $u_{\mathrm{max}}^{\mathrm{G,pul}}$ and the maximum stent movement $u_{\mathrm{max}}^{\mathrm{S,pul}}$ ($r_{\hat{q},\check{q}} = 0.89$).

In Figure 5, the coefficient of variation CVq (equation (35)) is considered for all EVAR quality parameters $q \in \mathcal{Q}$ at the nominal degree of SG oversizing of $o = 15\%$. In Appendix A4, the coefficient of variation CV$q(o)$ is continuously given over all degrees of SG oversizing in the range $o \in [5\%, 40\%]$. The coefficients of variation CVq over all $n^{\mathrm{Ao,diast}} = 61$ realizations and over all $n^{\mathrm{SG,diast}} = 13$ realizations are considered separately. $n^{\mathrm{Ao,diast}} = 61$ are all variations of the vessel parameters $g^{\mathrm{Ao}} \in \mathcal{G}^{\mathrm{Ao}}$ and $n^{\mathrm{SG,diast}} = 13$ are all variations of the SG parameters $g^{\mathrm{SG}} \in \mathcal{G}^{\mathrm{SG}}$ at the diastolic blood pressure state $p^{\mathrm{diast}} = 80$ mmHg. Hence, the coefficient of variation CVq over all $n^{\mathrm{Ao,diast}} = 61$ realizations (blue bars in Figure 5) indicates by how much the EVAR quality parameters $q \in \mathcal{Q}$ are influenced by the vessel parameters $g^{\mathrm{Ao}} \in \mathcal{G}^{\mathrm{Ao}}$ and the coefficient of variation CVq over all $n^{\mathrm{SG,diast}} = 13$ realizations (yellow bars in Figure 5) indicates by how much the EVAR quality parameters $q \in \mathcal{Q}$ are influenced by the SG parameters $g^{\mathrm{SG}} \in \mathcal{G}^{\mathrm{SG}}$.

According to Figure 5, the following EVAR quality parameters are strongly influenced by the vessel parameters $g^{\mathrm{Ao}} \in \mathcal{G}^{\mathrm{Ao}}$ with coefficients of variation CV$q > 0.35$ (blue bars in Figure 5): the maximum vessel relief $|\bar{\sigma}_1^{\lambda,\mathrm{wall}}|$, the SG drag force magnitude $||\boldsymbol{F}_{\mathrm{drag}}||$, the maximum stent-vessel gap $s_{\mathrm{max}}^{\mathrm{SA}}$ and the maximum stent movement $u_{\mathrm{max}}^{\mathrm{S,pul}}$. Further, the following EVAR quality parameters are strongly influenced by the SG parameters $g^{\mathrm{SG}} \in \mathcal{G}^{\mathrm{SG}}$ with coefficients of variation CV$q > 0.35$ (yellow bars in Figure 5): the maximum normal contact traction $t_{\mathrm{n},99}$, the maximum stent-vessel gap $s_{\mathrm{max}}^{\mathrm{SA}}$, the maximum conical stent shape $c_{\mathrm{max}}^{\mathrm{S}}$, the maximum graft movement $u_{\mathrm{max}}^{\mathrm{G,pul}}$ and the maximum stent movement $u_{\mathrm{max}}^{\mathrm{S,pul}}$.

3.2 | Influence of the degree of stent-graft oversizing

In Figure 6I, we qualitatively and quantitatively highlight the clear impact of the degree of SG oversizing o on the vessel overstress $\bar{\sigma}^{\mathrm{wall}}$. Furthermore, increased radial buckling associated with large local graft movements $\boldsymbol{u}^{\mathrm{G,pul}}$ can be identified for large degrees of SG oversizing (Figure 6II, black arrow).

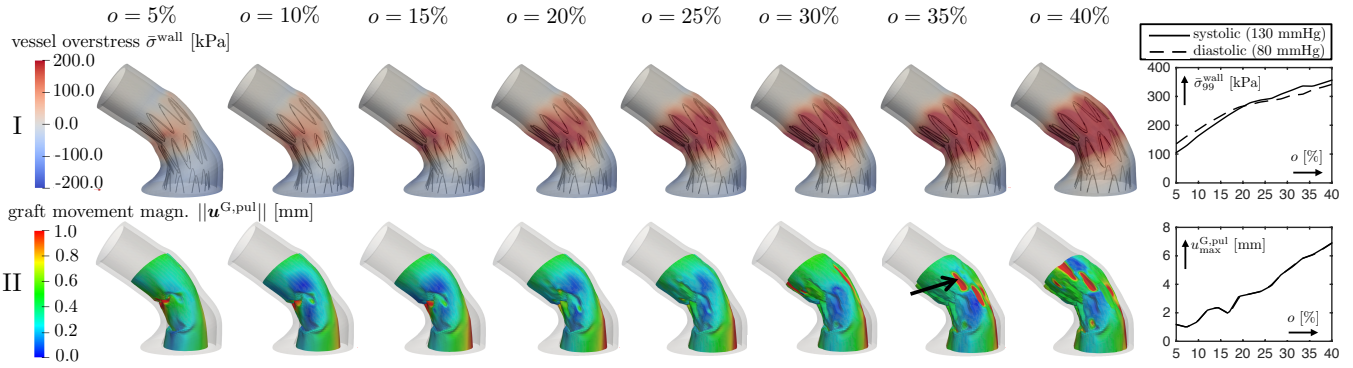

FIGURE 6 Visualization of the vessel overstress $\bar{\sigma}^{\text{wall}}$ (I), the magnitude of the graft movement $||\boldsymbol{u}^{\text{G,pul}}||$ (II) for different nominal degrees of SG oversizing o at the systolic pressure level of $p^{\text{sys}} = 130$ mmHg.

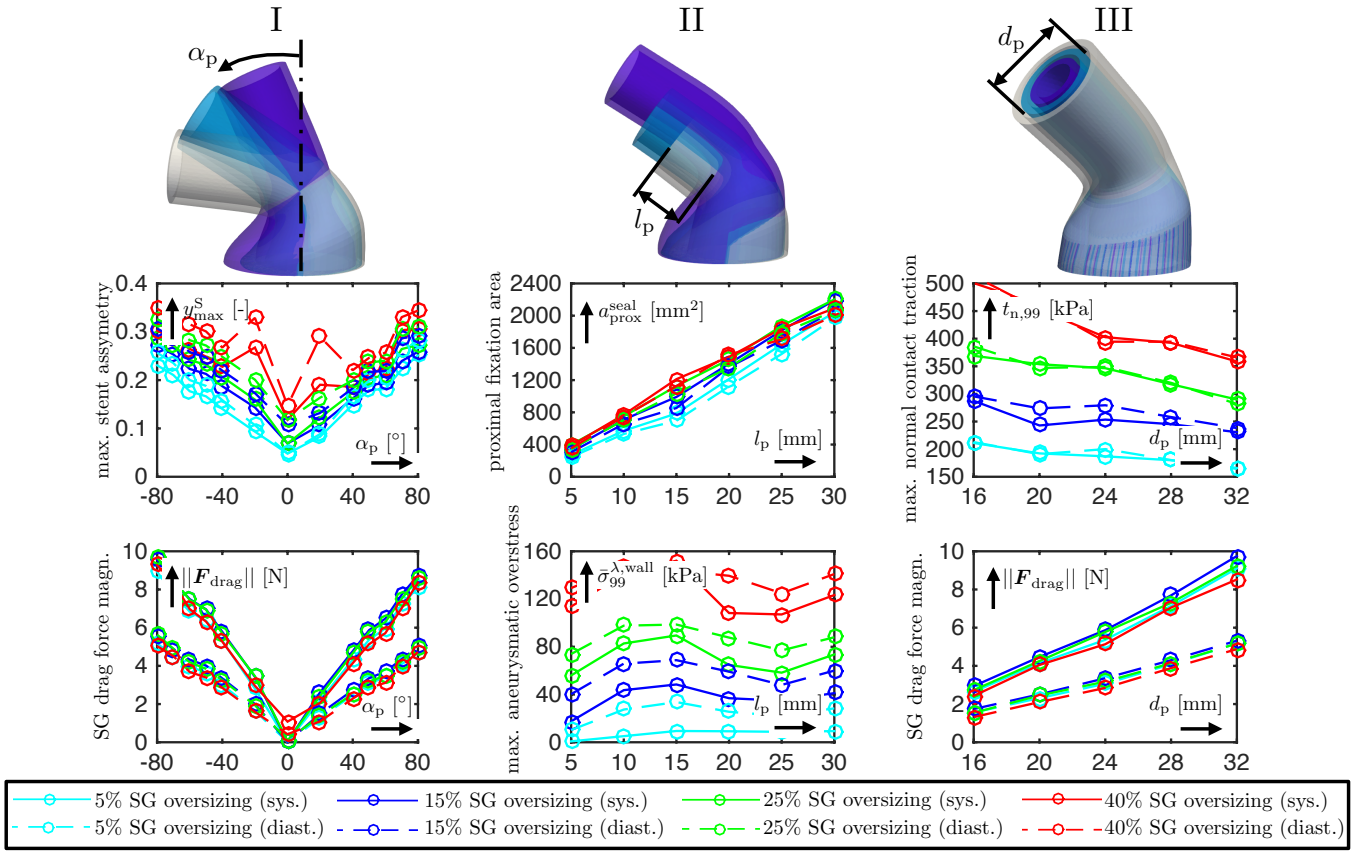

FIGURE 7 Influence of the proximal neck angle α_{p} (I) and the proximal neck length l_{p} (II) and the proximal neck diameter d_{p} (III) on selected EVAR quality parameters $q \in Q$ for different degrees of SG oversizing o as well as different blood pressure states $p^{\text{diast}} = 80$ mmHg and $p^{\text{sys}} = 130$ mmHg.

3.3 | Influence of vessel parameters

In Figure 7, some EVAR quality parameters are exemplarily shown for the variation of the proximal neck angle α_{p} (Figure 7I), the variation of the proximal neck length l_{p} (Figure 7II) and the proximal neck diameter d_{p} (Figure 7III).

Larger neck angles α_{p} lead both to a larger asymmetry $y^{\text{S}}_{\text{max}}$ of the stent rings in the curved region of the vessel and to a substantially increase in the SG drag force magnitude $\boldsymbol{F}_{\text{drag}}$ (Figure 7I). Qualitative investigations of those two findings are

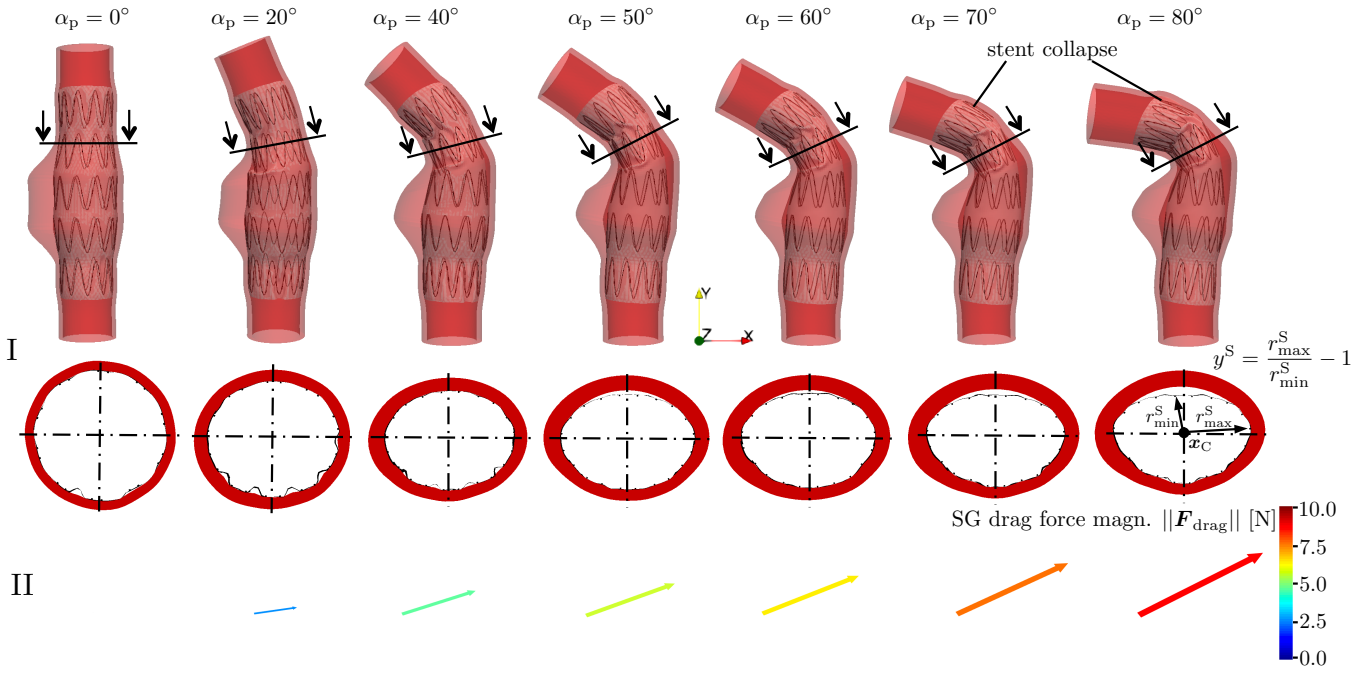

FIGURE 8 Visualization of the stent asymmetry y^S (I) and the SG drag force F_{drag} (II) for different proximal neck angles α_p with a nominal SG oversizing of $o = 15\%$ at the systolic pressure level of $p^{sys} = 130$ mmHg.

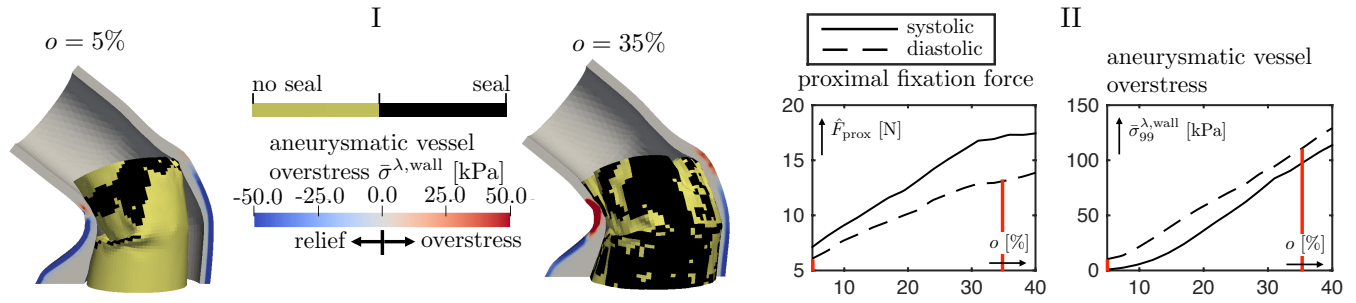

FIGURE 9 Qualitative comparison of the quality of seal and the aneurysmatic vessel overstress (I) as well as quantitative comparison of the proximal SG fixation force $\hat{F}_{prox}$ and the aneurysmatic vessel overstress $\sigma^{\lambda,wall}_{99}$ of a SG oversized by $o = 5\%$ and a SG oversized by $o = 35\%$ in a vessel with short proximal neck length $l_p = 5$ mm at the diastolic blood pressure state $p^{diast} = 80$ mmHg.

provided in Figure 8 for proximal neck angles in the range $\alpha_p = [0°; 80°]$. Additionally, in Figure 8I, stent collapse is visible for the deployed SG in vessels with a neck angle of $\alpha_p \geq 70°$.

A short neck length l_p causes a small fixation area a^{seal}_{prox} (Figure 8II) associated with a relatively poor quality of seal as well as small fixation forces $\hat{F}_{prox}$ (Figure 9). Increasing the degree of SG oversizing o might be one potential way of improving the quality of seal and the fixation forces in a vessel with short neck length l_p. The downside of this approach is visualized in Figure 9 by comparing the results of a SG oversized by $o = 5\%$ and a SG oversized by $o = 35\%$ in the vessel with short neck length $l_p = 5$ mm. A larger degree of SG oversizing improves the quality of seal and the fixation forces of the SG. However at the expense of increased aneurysmatic vessel overstresses in the AAA shoulder region which might trigger negative effects such as ongoing AAA growth in this region. Hence, at the expense of the potential long term durability.

The magnitude of SG drag forces $||F_{drag}||$ increases approximately linearly with increasing neck diameter d_p since the luminal area on which the blood pressure acts increases approximately linearly with increasing neck diameter d_p (Figure 7III). Although

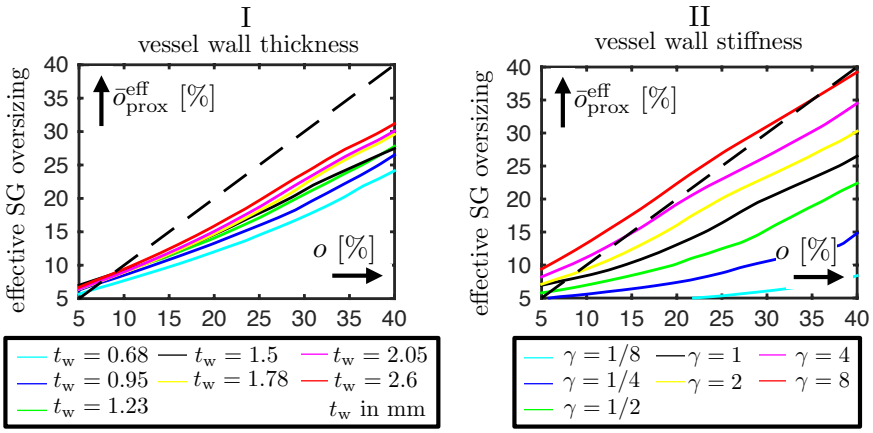

FIGURE 10 Investigation of vessel uncertainties at $p^{\text{sys}} = 130$ mmHg: influence of the vessel wall thickness t_w (I) and the vessel wall stiffness γ (II) on the effective degree of SG oversizing $\bar{o}^{\text{eff}}_{\text{prox}}$ for different nominal degrees of SG oversizing o. Dashed line indicates reference of $o = \bar{o}^{\text{eff}}_{\text{prox}}$.

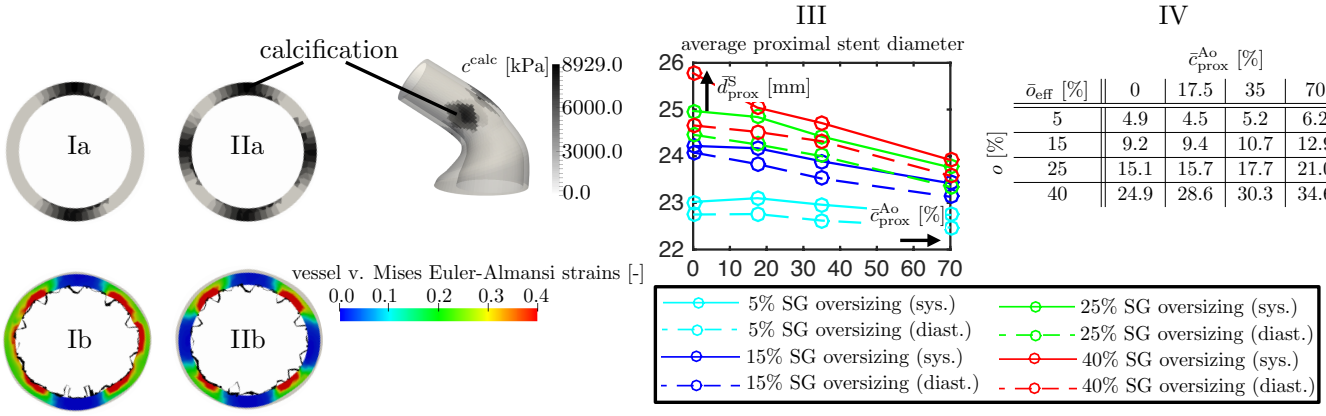

FIGURE 11 Influence of vessel calcifications in the proximal landing zone: visualization of the calcification spots of the vessel with two calcified spots (Ia) and the vessel with four calcification spots (IIa). Visualization of the vessel von Mises Euler-Almansi strains for a vessel with two calcification spots (Ib) and a vessel with four calcification spots (IIb); in grey: visualization of the deformed vessel without calcifications (Ib, IIb). Average proximal stent expansion diameter $\bar{d}^{\text{S}}_{\text{prox}}$ plotted over the percentage circumferential proximal neck calcification $\bar{c}^{\text{Ao}}_{\text{prox}}$ for different degrees of SG oversizing and different blood pressure states (III). Effective degree of SG oversizing $\bar{o}_{\text{eff}}$ for different degrees of percentage circumferential proximal neck calcification $\bar{c}^{\text{Ao}}_{\text{prox}}$ and different nominal degrees of SG oversizing o at $p^{\text{sys}} = 130$ mmHg (IV).

the sealing area between SG and vessel increases as well with increasing neck diameter d_p, the fixation force $\hat{F}_{\text{prox}}$ does not substantially increase with increasing d_p since simultaneously the normal contact tractions between SG and vessel decrease (Figure 7III). Hence, vessels with a larger neck diameter d_p might be rather prone to SG migration since the drag-fixation ratio of the SG is worse.

The following vessel uncertainties are investigated in this study: the vessel wall thickness t_w (Figure 10I) and the vessel wall stiffness γ (Figure 10II) according to equation (3). In Figure 10I+II, the effective degree of SG oversizing $\bar{o}^{\text{eff}}_{\text{prox}}$ is plotted against the nominal degree of SG oversizing o for vessel walls of different thickness t_w and vessel walls of different stiffness γ. The softer and the thinner the vessel wall, the larger is the immediate postimplant vessel dilatation and hence the larger is the difference between nominal and effective degree of SG oversizing. In the case of the very stiff vessel ($\gamma = 8$, red curve in Figure 10II), the SG induced vessel deformation is very small. Hence the local stent expansion diameter $\bar{d}^{\text{S}}(s_{\text{De}})$ is approximately equivalent to the preinterventional vessel diameter d_p. Consequently, the nominal and the effective degree of SG oversizing are approximately

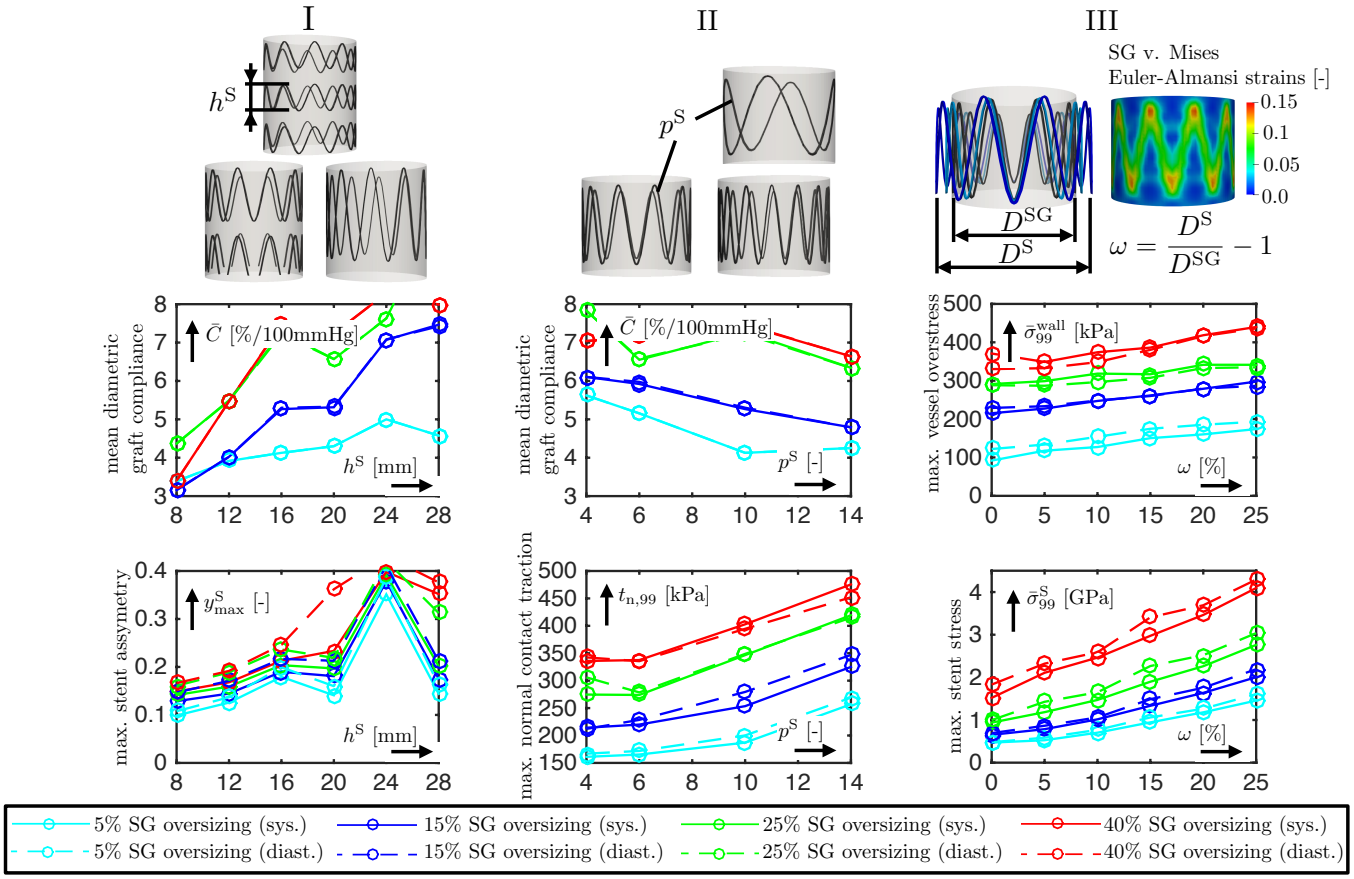

FIGURE 12 Influence of the stent height h^S (I), the number of periods per stent limb p^S(II) and the degree of stent predeformation ω (III) on selected EVAR quality parameters $q \in \mathcal{Q}$ for different degrees of SG oversizing o as well as different blood pressure states $p^{diast} = 80$ mmHg and $p^{sys} = 130$ mmHg.

the same (cf. equation (5) and (25)):

$$o_{eff}(s_{De}) = \frac{D^{SG}}{\bar{d}^S(s_{De})} - 1 \approx \frac{D^{SG}}{d_p} - 1 = o \tag{40}$$

In contrast to the stiff vessel, the soft vessel ($\gamma = 1/8$, cyan curve in Figure 7V) exhibits enormous immediate postimplant SG induced vessel dilatation such that the stent almost fully expands and the local stent expansion diameter $\bar{d}^S(s_{De})$ is close to the nominal diameter D^{SG} of the SG. Hence,

$$o_{eff}(s_{De}) = \frac{D^{SG}}{\bar{d}^S(s_{De})} - 1 \approx \frac{D^{SG}}{D^{SG}} - 1 = 0. \tag{41}$$

In Figure 11, the influence of vessel calcifications in the proximal landing zone is investigated. The difference in the stent expansion diameter $\bar{d}^S_{prox}$ of the stent in the proximal landing zone between a non-calcified aortic neck ($\bar{c}^{Ao}_{prox} = 0$ %) and a highly calcified aortic neck ($\bar{c}^{Ao}_{prox} = 70$ %) seems to be small (Figure 11III). However, considering the effective degree of SG oversizing $\bar{o}^{eff}_{prox}$, this difference might be very essential. Having in mind that in clinical practice a nominal degree of SG oversizing of $o \in [10\,\%, 20\,\%]$ is aspired, a difference in 3.7 % effective SG oversizing $\bar{o}_{eff}$ between the highly calcified ($\bar{c}^{Ao}_{prox} = 70$ %) and the non-calcified aortic neck ($\bar{c}^{Ao}_{prox} = 0$ %) is substantial (Figure 11IV, $o = 15\%$).

3.4 | Influence of stent-graft parameters

To keep the total SG length L^{SG} and the length of the gap between stent limbs constant over all considered variations of the stent height h^S, we adapted the number of stent limbs n^S of the SG. SGs with many short stent limbs are radially stiffer than SGs with few long stent limbs. Hence, the mean diametric graft compliance $\bar{C}$ increases with increasing stent height h^S (Figure 12I and

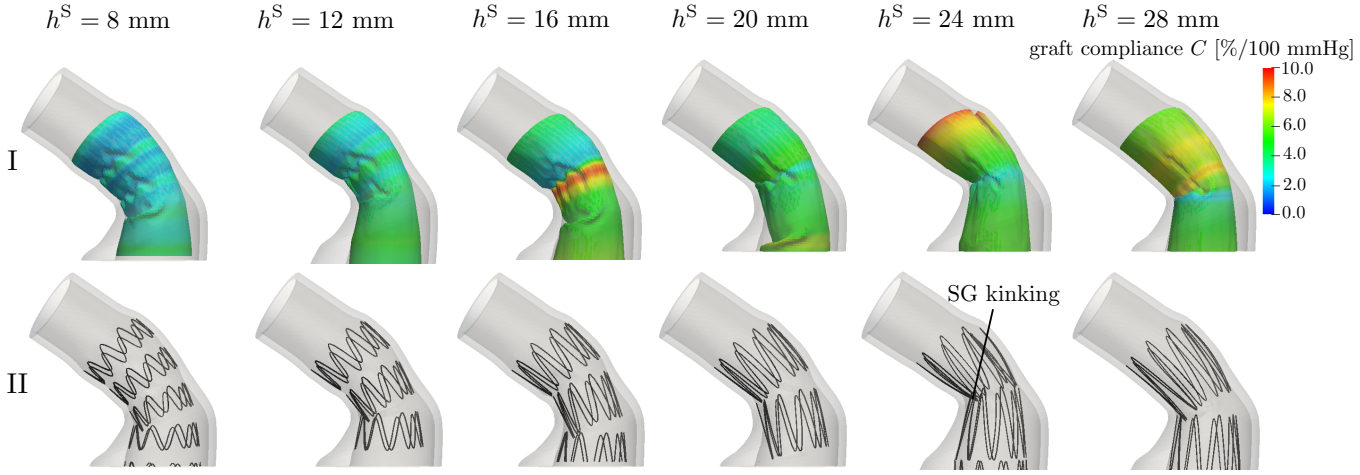

FIGURE 13 Visualization of the diametric graft compliance C (I) and the deployed stent configuration (II) for different stent heights h^S for a SG oversized by $o = 15\%$ at the systolic pressure level of $p^{sys} = 130$ mmHg. Clearly visible SG kinking in the case of $h^S = 24$ mm.

Figure 13I). Further, SGs with shorter stent limbs, i.e. smaller h^S, are more flexible and can better adapt to the curved vessel geometry. Hence, SGs with stent limbs of large height h^S have an increased tendency to SG kinking with its associated negative effects in tortuous vessels. However, whether there will be SG kinking or not also strongly depends on the position of the single stent limbs in the curved regions of the vessel. For the given vessel geometry, a SG with $h^S = 24$ mm shows considerable SG kinking whereas a SG with $h^S = 28$ mm does not show any SG kinking (Figure 13II). Increased stent asymmetry y^S_{max} is a side effect of the increased tendency to SG kinking. SG kinking occurs at the gaps between stent limbs. The deformation of the adjacent stent limbs is large in case of SG kinking leading to an ovalization of the stent limbs, i.e. to large stent asymmetries y^S_{max} (Figure 12I).

SGs with stent limbs that have a larger number of periods p^S per stent limb behave radially stiffer. Hence, increasing the number of periods p^S per stent limb leads to a reduction of the mean diametric compliance $\bar{C}$ of the SG (Figure 12II). Further, a larger number of periods p^S per stent limb causes higher contact tractions $t_{n,99}$ and fixation forces $\hat{F}_{prox}$ between SG and vessel. This effect is likewise for all considered degrees of SG oversizing o (Figure 12II).

While positive effects of stent predeformation ω on the radial buckling of the graft and the SG fixation were reported for instance in[32], in Figure 12III we explicitly show some downsides of stent predeformation. Larger degrees of stent predeformation ω result in higher vessel overstresses $\bar{\sigma}^{wall}$. Further, especially in combination with large degrees of SG oversizing o, large degrees of stent predeformation ω lead to very high stent stresses σ^S.

3.5 | Influence of the arterial blood pressure

In Figure 14, the relative influence of the blood pressure state on the EVAR quality parameters $q \in \mathcal{Q}$ is investigated where the relative change of the EVAR quality parameter Δq is given by

$$\Delta q(o) = \frac{\mu_q^{sys}(o) - \mu_q^{diast}(o)}{\mu_q^{diast}(o)}, \quad \forall q \in \mathcal{Q} \tag{42}$$

In equation (42), μ_q^{sys} is the mean value of the EVAR quality parameter q at the systolic blood pressure state of $p^{sys} = 130$ mmHg and μ_q^{diast} is the mean value of the EVAR quality parameter at the diastolic blood pressure state of $p^{diast} = 80$ mmHg (equation (36)). This consideration gives some insight whether the diastolic or whether the systolic blood pressure state is more crucial for the EVAR quality parameter $q \in \mathcal{Q}$.

In Figure 14, the influence of the arterial blood pressure state Δq is plotted for a nominal degree of SG oversizing of $o = 15\%$. In Appendix A4, the influence of the arterial blood pressure state $\Delta q(o)$ is continuously given over all degrees of SG oversizing in the range $o \in [5\%, 40\%]$. Figure 14 highlights that some EVAR quality parameters are larger at the systolic blood pressure

state ($\Delta q > 0$) while others are larger at the diastolic blood pressure state ($\Delta q < 0$). The following EVAR quality parameters are strongly influenced by the blood pressure state with $|\Delta q| > 50\%$: the maximum vessel relief $|\bar{\sigma}_1^{\text{wall}}|$ and the magnitude of the SG drag forces $||\boldsymbol{F}_{\text{drag}}||$.

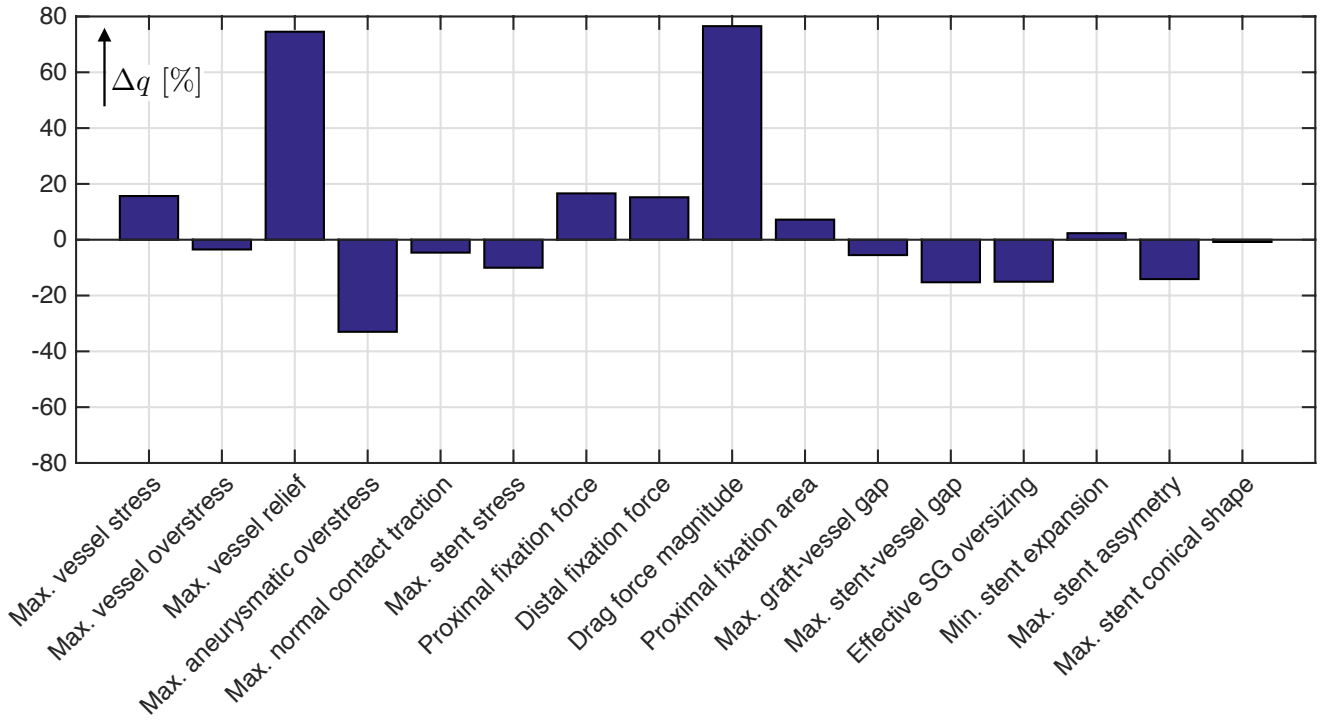

FIGURE 14 Influence of the arterial blood pressure state Δq according to equation (42) on EVAR quality parameter q at a nominal degree of SG oversizing of $o = 15\%$. A value of $\Delta q > 0$ indicates that the EVAR quality parameter q is larger in the systolic blood pressure state $p^{\text{sys}} = 130$ mmHg whereas a value of $\Delta q < 0$ indicates that the EVAR quality parameter q is larger in the diastolic blood pressure state $p^{\text{diast}} = 80$ mmHg.

Having a closer look on the results visualized in Figure 14, several interesting impacts of the blood pressure state can be observed. It is plausible that the vessel relief $|\bar{\sigma}_1^{\text{wall}}|$, which describes the reduction of the vessel wall stresses in the "diseased" region of the aneurysm sac, is much larger in the systolic than in the diastolic blood pressure state. This is because the preinterventional vessel stresses in the aneurysm sac are larger in systolic pressure state. Hence, the difference between the preinterventional vessel stresses and the postinterventional vessel stresses in the aneurysm sac are larger (cf. equation (14)) having in mind that the postinterventional vessel stresses in the aneurysm sac are close to zero for most of the considered $n = 146$ realizations independent of the blood pressure state. Both, SG fixation forces $\hat{F}_{\text{prox}}$ and $\hat{F}_{\text{dist}}$ as well as the magnitude of the SG drag forces $||\boldsymbol{F}_{\text{drag}}||$ are larger at the systolic blood pressure state ($\Delta q > 0$). Since the influence of the blood pressure on the drag force $\boldsymbol{F}_{\text{drag}}$ is much larger than on the fixation forces $\hat{F}_{\text{prox}}$ and $\hat{F}_{\text{dist}}$, the risk of SG migration might be higher at the systolic pressure state. Furthermore, maximum stent stresses σ_{99}^{S} are around 10% larger in the diastolic than in the systolic blood pressure state ($\Delta q \approx -10\%$) since the SG in the deployed state in the landing zones, i.e. in the regions where mostly the largest stent stresses occur, is under compression. Hence, an increase of arterial blood pressure relaxes the SG in the landing zones. The proximal fixation area $a_{\text{prox}}^{\text{seal}}$ is larger at the systolic blood pressure state ($\Delta q > 0$) whereas the maximum graft-vessel gap $s_{\text{max}}^{\text{GA}}$ and the maximum stent-vessel gap $s_{\text{max}}^{\text{SA}}$ in the proximal landing zone are larger in the diastolic blood pressure state ($\Delta q < 0$). The main reason for this finding is that the larger the blood pressure, the more the SG is pressed against the vessel. Hence, the fixation area $a_{\text{prox}}^{\text{seal}}$ increases whereas the graft-vessel gap $s_{\text{max}}^{\text{GA}}$ and the stent-vessel gap $s_{\text{max}}^{\text{SA}}$ decrease with increasing blood pressure. As a consequence, the risk of leakage might be higher at the diastolic blood pressure state.

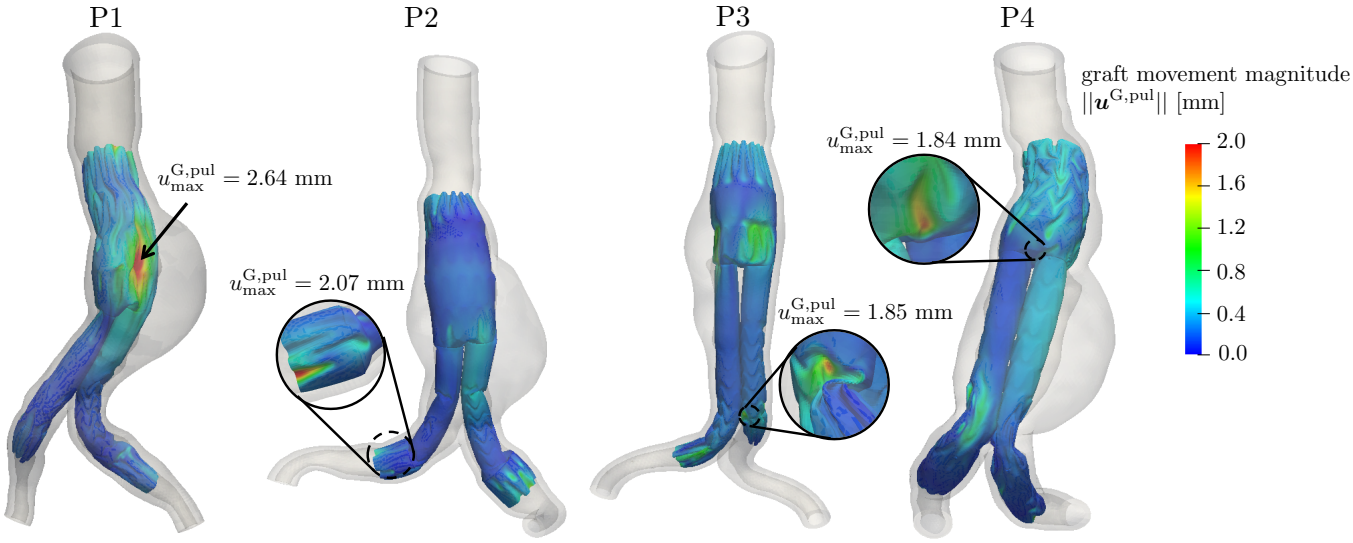

FIGURE 15 Visualization of the magnitude of the graft movement $||\boldsymbol{u}^{\mathrm{G,oul}}||$ of four patient-specific cases. Patient P1-P3 were treated by Cook Zenith Flex/Spiral-Z® SGs. Patient P4 was treated by a Medtronic Endurant™ II SG. Circles with dashed lines indicate detail on the backside of the SG.

3.6 | Application to patient-specifc cases

In this section we show the applicability of the use of the EVAR quality parameters $q \in \mathcal{Q}$ to patient-specific cases and compare the obtained values to the ones of the parameterized, synthetic vessels and SGs. We consider three patient-specific cases treated by Cook Zenith Flex/Spiral-Z® SGs and one patient treated by a Medtronic Endurant™ II SG (Figure 15). Material models and model parameters of the patient-specific SGs and vessels are taken from[33]. The objective of this section is rather to show the applicability than providing a full investigation of the four patient-specific cases. Hence, the interested reader is referred to the original publication[33] for information on the geometrical parameters of the patient-specific vessels and SGs. Further, only selected EVAR quality parameters $q \in \mathcal{Q}$ are investigated in Figure 15 and Table 3.

In Figure 15, the magnitude of graft movement $||\boldsymbol{u}^{\mathrm{G,pul}}||$ during one heart beat is shown exemplarily for the four patients. Maximum values of $||\boldsymbol{u}^{\mathrm{G,pul}}||$ occur at local folds in all four patient-specific cases. However, the location of the local folds with maximum movement $u_{\max}^{\mathrm{G,pul}}$ is different for each patient-specific case.

In Table 3, a comparison between the parameterized, synthetic vessels and SGs and the four patient-specific cases is given for selected EVAR quality parameters $q \in \mathcal{Q}$. Values with yellow background in Table 3 are within $\mu_q(o = 15\%) \pm \sigma_q(o = 15\%)$ of the parameterized, synthetic vessels and SGs at a reasonable degree of SG oversizing of $o = 15\%$. μ_q and σ_q are the mean and the standard deviation over all $n^{\mathrm{sys}} = 73$ considered realizations of the synthetic vessel at $p^{\mathrm{sys}} = 130$ mmHg according to equation (36) and (37), respectively. Values with green background are smaller than $\mu_q(o = 15\%) - \sigma_q(o = 15\%)$ and values with red background are larger than $\mu_q(o = 15\%) + \sigma_q(o = 15\%)$. The maximum vessel wall overstresses $\bar{\sigma}_{99}^{\mathrm{wall}}$ of three of the four patients are larger than the values of the parameterized, synthetic vessels and SGs at a nominal degree of SG oversizing of $o = 15\%$. The main reason is that the nominal degree of SG oversizing o of all four patient-specific cases is larger than 15% which is used for comparison in Table 3. This is also visible in the effective degree of SG oversizing $o_{\mathrm{prox}}^{\mathrm{eff}}$ of all four patient-specific cases which is larger than the effective degree of SG oversizing of the reference of the parameterized, synthetic vessels and SGs. A larger degree of SG oversizing results in higher vessel stresses as shown in Section 3.2. The aneurysmatic vessel wall overstresses $\bar{\sigma}_{99}^{\lambda,\mathrm{wall}}$ strongly depend on the location of the landing zone of the SG. If the SG landing zone is partly in an "aneurysmatic" part of the vessel (patients P1 and P4), the aneurysmatic vessel wall overstresses $\bar{\sigma}_{99}^{\lambda,\mathrm{wall}}$ can be very high. In contrast, if the SG landing zone is fully in the "healthy" part of the vessel (patients P2 and P3), the aneurysmatic vessel wall overstresses $\bar{\sigma}_{99}^{\lambda,\mathrm{wall}}$ are close to zero. The maximum vessel relief $|\bar{\sigma}_{1}^{\lambda,\mathrm{wall}}|$ of the patient-specific cases P2-P4 are in the range of the reference of the parameterized, synthetic vessels and SGs. In case of the patient-specific case P1, the luminal diameter in the aneurysm sac is small due to a relatively thick ILT layer. As a consequence, the SG is almost fully in contact with the ILT in the aneurysm sac which prevents the reduction of the vessel stresses in the aneurysm sac after the insertion of the SG. Hence, the

TABLE 3 Quantitative evaluation of the deployed SG configurations of the four patient specific cases with respect to selected EVAR quality parameters at the systolic pressure state of $p^{sys} = 130$ mmHg. Colors indicate amount of the value of the EVAR quality parameter $q \in Q$ in relation to the values of the parameterized, synthetic vessels and SGs at $o = 15\%$ SG oversizing.

$q \in Q$	$\bar{\sigma}_{99}^{wall}$	$\bar{\sigma}_{99}^{\lambda,wall}$	$\lvert\bar{\sigma}_{1}^{\lambda,wall}\rvert$	a_{prox}^{seal}	o_{prox}^{eff}	$u_{max}^{G,pul}$	$\bar{C}$
dim	[kPa]	[kPa]	[kPa]	[mm^2]	[%]	[mm]	$[\frac{\%}{100\ mmHg}]$
P1	467	84.8	13.8	521	34.5	2.64	4.98
P2	238	4.7	132	786	16.3	2.07	3.17
P3	303	20.2	85.9	632	23.0	1.85	3.68
P4	370	55.9	114	474	14.5	1.84	3.13

$q < \mu_q^{15} - \sigma_q^{15}$; $\mu_q^{15} - \sigma_q^{15} \leq q \leq \mu_q^{15} + \sigma_q^{15}$; $q > \mu_q^{15} + \sigma_q^{15}$

$\mu_q^{15} = \mu_q(o = 15\%)$; $\sigma_q^{15} = \sigma_q(o = 15\%)$ (equation (36) and (37))

maximum vessel relief $\lvert\bar{\sigma}_{1}^{\lambda,wall}\rvert$ is smaller for this patient. The proximal fixation area a_{prox}^{seal} is smaller for all four patient-specific cases than the mean value of the parameterized, synthetic vessels and SGs. One possible explanation for this observation are the nonuniform vessel shapes of the patient-specific vessels and the associated reduced attachment to the vessel at certain locations in the proximal landing zone. In contrast, the synthetic vessels have perfectly circular vessel cross sections that perfectly fit to the cylindrical shape of the SG. The maximum graft movement $u_{max}^{G,pul}$ of all four patient-specific cases is in the range of the values of the parameterized, synthetic vessels and SGs at a nominal degree of SG oversizing of $o = 15\%$. The mean diametric graft compliance $\bar{C}$ is smaller for most of the bifurcated SGs of the patient-specific cases compared to the reference of the parameterized, synthetic vessels and SGs. In contrast to the parameterized SG as presented in Section 2.3, the bifurcated SGs of the patient-specific cases have two long iliac SG components. These iliac SG components have a much smaller diameter and are radially stiffer than the parameterized SG. Hence, the mean diametric graft compliance $\bar{C}$ of the bifurcated SGs is smaller.

4 | SUMMARY OF THE RESULTS AND DISCUSSION

In the present work, a fully parameterized AAA and SG geometry was developed. A parameter study was performed on in total $n = 146$ different realizations of the vessel and SG parameters by using an in silico EVAR approach[32]. In the parameter study, the degree of SG oversizing was treated as continuous variable between 5% and 40% oversizing by using a SG parameter continuation approach[32]. 20 EVAR quality parameters were defined to assess the outcome of the in silico EVAR approach with respect to complication likelihoods such as SG migration, endoleaks or aortic neck dilatation.

The following impacts of SG oversizing could be identified:

- Vessel and stent stresses increase with increasing degree of SG oversizing.
- SG fixation forces and maximum normal contact tractions between SG and vessel increase with increasing degree of SG oversizing.
- SG drag force not substantially affected by the degree of SG oversizing.
- For large degrees of SG oversizing the effective SG oversizing is clearly smaller than the nominal SG oversizing since the SG induced immediate postimplant vessel dilatation[77] reduces the effective degree of SG oversizing.
- Increased SG oversizing leads to increased radial buckling of the SG. Locally large relative movements of the resulting folds are possible every heart beat which could have negative effects on the fatigue behavior of the graft.

Substantially increased vessel stresses when using high degrees of SG oversizing might have negative effects on the longevity of EVAR. Both, high vessel overstresses as well as high aneurysmatic vessel overstresses might induce growth and remodeling

of the vessel after EVAR and lead to aortic neck dilatation. But the way of how the two quantities might trigger growth and remodeling is different. Aneurysmatic vessel overstresses might strengthen ongoing aneurysm growth of the already diseased ”aneurysmatic“ vessel material and hence change the sealing zone[21,79]. In contrast to that, vessel overstresses might trigger growth and remodeling of ”healthy“ vessel material in the sealing zones and hence also lead to aortic neck dilatation and associated reduced longevity of EVAR[62]. Both, phenomena are widely discussed in literature but without full agreement of the major source of aortic neck dilatation[89,17,88].

There are numerous different stent designs of marketed SGs. In this study, we showed the impact of stent design parameters on the EVAR outcome which led to the following findings:

- A large number of periods per stent limb, i.e. a large number of loops of the sinusoidally shaped stent limb, leads to radially stiffer SGs with reduced SG compliacnce.
- SGs with shorter stent limbs are more flexible and lead to a better SG-vessel attachment with reduced risk of SG kinking.
- Excessive stent predeformation can result in high stent stresses. Especially, if used in combination with a large degree of SG oversizing.
- None of the investigated SG designs showed significant aortic compliance mismatch. The mean diametric graft compliance was largely in the range of reported values of healthy abdominal aortas ($3.7 - 6.8\ \%/100$ mmHg)[43].

Variations of vessel parameters showed the following major impacts of the vessel geometry on the EVAR outcome:

- Vessel uncertainties[7], such as the vessel wall thickness and vessel wall stiffness, have a substantial impact on the effective degree of SG oversizing.
- The local stiffening of the vessel by calcifications leads to reduced SG expansion and a higher degree of effective SG oversizing.
- The neck angle has a very large impact on the SG drag force as often stated in literature[46,22].
- Short neck length has the most negative impact on SG fixation as also stated for instance by[95,2].
- The magnitude of SG drag forces increases almost linearly with increasing neck diameter since the luminal area on which the blood pressure acts increases approximately linearly with increasing neck diameter.

The last point is in accordance with several studies that mention an increase in SG drag forces and an increased risk of SG migration for patients with large vessel diameters[63,45,60,56]. In contrast to the SG drag force, the SG fixation force is little affected by the neck diameter. This observation however is limited by the fact that in the current parameter study, the number of periods per stent limb was kept constant when increasing the SG diameter. However, SGs with larger diameter might require a larger number of periods per stent limb which would increase the radial stiffness of the SG.

The problematic nature of hostile necks[4,1,37], such as high angulation and short neck length, could clearly be shown in the parameter study. Higher degrees of SG oversizing in the case of hostile necks showed to be a possibility to counteract small fixation areas and small SG fixation forces as suggested in some medical and experimental studies[88,89,10].

Even if the diameter of the deployed SG is little affected by the blood pressure state[33], investigations of the EVAR outcome at the diastolic blood pressure state of 80 mmHg and at the systolic pressure state of 130 mmHg have shown that it is important to consider both blood pressure states to assess the quality of the EVAR outcome. Some EVAR quality parameters are critical in the diastolic state while others are critical in the systolic state. The most non-intuitive findings of the consideration of different blood pressure states are:

- Maximum vessel overstresses, i.e. the difference in vessel stresses before and after EVAR, are larger in the diastolic blood pressure state.
- Maximum stent stresses are around 10% larger in the diastolic than in the systolic pressure state since a larger blood pressure reduces the compression of the stent in the landing zone and hence relaxes the stent.
- In the diastolic blood pressure state, the gap between SG and vessel is larger which increases the risk of leakage.

- The SG drag force is approximately 80% larger in the systolic blood pressure state which is in accordance with the frequently stated increased risk of SG migration in case of hypertension[46,60,56].

Furthermore, the increase of the SG drag force magnitude of approximately 80% is larger than the assumed systolic-diastolic pressure ratio of $\frac{130\ \text{mmHg}}{80\ \text{mmHg}} - 1 = 62.5\%$ which indicates nonlinear effects on the evaluation of SG drag forces. Assuming rigid SGs and rigid vessels, as done in many studies investigating the SG drag force[34,56,24], would lead to 62.5% larger drag forces in the systolic state than in the diastolic state as long as shear tractions are neglected in the computation of the SG drag force. This is because in case of a rigid SG and rigid vessel the integration area of the luminal graft surface does not change between diastolic and systolic pressure state. Hence, the SG drag force is only scaled by the internal pressure state p (equation (16)). Considering an elastic SG and vessel, as in this study, a pressure increase leads also to an increase of the the integration area of the luminal graft surface γ_1^{G}. Hence, the SG drag force increase is larger than the assumed systolic-diastolic pressure ratio of 62.5%. Consequently, such an rigidity assumption potentially underestimates the SG drag force.

Finally, it was shown that all presented methods are applicable to patient-specific cases.

5 | LIMITATIONS

In the present study, we used an in silico EVAR approach to approximate the deployed state of SG and vessel which is a strongly simplified process compared to the real-world medical intervention. The in vivo deployed SG configuration might depend on many interventionalist-specific factors that are not considered in the in silico approach such as the speed of SG deployment and the application of a molding angioplasty to further unfold the SG.

Although the definition of a successful EVAR intervention was defined as being complication-free for several years after the intervention, we did not consider any growth and remodeling which would be required to consider the development of the EVAR quality parameters over several years. In the present study, all EVAR quality parameters are quantities taken directly after the SG deployment.

Furthermore, we used an extremely simplified approach to investigate patient-specific uncertainties which did not consider intrapatient variability of vessel wall thickness and vessel wall stiffness but used spatially constant parameters. The major intention was to show the potential impact of these patient-specific uncertainties on the EVAR outcome.

To get a full understanding of the influence of the geometrical vessel and SG parameters and their potential interplay on the EVAR outcome a full factorial parameter study would be necessary. However, a full factorial analysis for the given number of parameters and number of parameter variations is computationally not achievable. Therefore, we used a basic vessel and SG geometry from which single parameters were modified while all others were kept constant. Choosing a different basic vessel and SG geometry might slightly change the outcome.

In the present study, the focus was put on quantitative evaluation of the EVAR outcome. However, a pure quantitative assessment might lead to misinterpretations in certain cases. For instance, a high value of the proximal fixation area does not necessarily mean that this is a leak-proof seal. Instead, the SG could be well attached just on one side, but an endoleak occurs on the averted side.

The parameter study of the synthetic vessel and SG as well as the consideration of four patient-specific cases revealed mean values, standard deviations and expectable ranges of the single EVAR quality parameters that can be used for comparisons. However, no statement about ranges in which the parameters are acceptable or not could be made. To determine these ranges of the EVAR quality parameters in which the EVAR outcome is acceptable, i.e. the EVAR outcome is free of complications, a much larger cohort of patient-specific cases has to be evaluated and statistically investigated with respect to EVAR complications.

Having achieved such a clear link between EVAR complications and EVAR quality parameters with ranges of acceptable values for the EVAR quality parameters, the IFU could be formulated in terms of mechanical and geometrical parameters that are based on the predicted deployed SG configuration such as the presented EVAR quality parameters. Such IFU based on mechanical and geometrical parameters of the predicted deployed SG configuration should outline the limits of the applicability of EVAR much better than the current IFU that are based on the preinterventional vessel geometry.

6 | CONCLUSIONS

This study confirmed the hypothesis that the outcome of EVAR is strongly dependent on vessel and SG parameters. Candidates with high risk of postinterventional complications are in particular patients with a large neck angle, a large vessel diameter, a short neck length as wells as soft and thin vessel walls. It was shown that the degree of SG oversizing has a decisive role on the EVAR outcome and hence might have a big impact on the likelihood of postinterventional complications.

The complexity of decision making whether a patient is a promising candidate for EVAR demands a new definition of the IFU. IFU that are not only based on geometrical parameters of the preinterventional vessel geometry but mainly use mechanical and geometrical parameters of the predicted deployed SG configuration to assess the EVAR complication likelihood should outline the limits of the applicability of EVAR much better.

In this study, the EVAR outcome was evaluated with respect to 20 parameters that quantify the mechanical state and the geometrical shape of SG and vessel after the in silico SG deployment. A comparison of the EVAR outcome at the diastolic and the systolic blood pressure state showed the importance of considering both blood pressure states to assess the quality and complication likelihood of the EVAR outcome. While some parameters, such as the maximum stent stresses, are larger at the diastolic blood pressure state other parameters, such as the SG drag force, are crucial at the systolic blood pressure state.

The definition of these mechanical and geometrical parameters and their extensive investigation established the basis for the development of a predictive tool to assess the potential success of EVAR in a clinical setting. The next step is the construction of a simulation based metric which incorporates these mechanical and geometrical parameters to predict the complication likelihood of EVAR and which is easily interpretable by a clinician.

7 | ACKNOWLEDGEMENTS

The authors gratefully acknowledge support and funding by the Leibniz Rechenzentrum München (LRZ) of the Bavarian Academy of Sciences under contract number pr48ta.

8 | CONFLICT OF INTEREST

All authors declare that no conflicts of interest exist.

APPENDIX A1: CONSTITUTIVE MODELING

In Table 4, the constitutive models and material parameters of vessel wall, ILT, calcifications and SG are summarized.

APPENDIX A2: MESH CONVERGENCE STUDY

The mesh convergence is proven for the SG and vessel described by the basic parameters $\hat{g} \in \mathcal{G}$ provided in Table 2. In Figure 16, the mean stent limb diameters $\overline{\bar{d}^{\mathrm{S}}}$ of the five stent limbs in the deployed state are investigated for different discretizations of vessel and SG. The mean stent limb diameter $\overline{\bar{d}^{\mathrm{S}}}$ is given by

$$\overline{\bar{d}^{\mathrm{S}}} = \frac{1}{h^{\mathrm{S}}_{\mathrm{De}}} \int_{s_0}^{s_1} \bar{d}^{\mathrm{S}}(s_{\mathrm{De}}) \mathrm{d}s_{\mathrm{De}}, \tag{43}$$

where $h^{\mathrm{S}}_{\mathrm{De}}$ is the stent limb height in the deployed state, s_0 describes the location of the most proximal point of the stent limb, s_1 is the location of the most distal point of the stent limb and $\bar{d}^{\mathrm{S}}(s_{\mathrm{De}})$ is the average stent diameter in an orthogonal slice at the location s_{De} as described in section 2.4.4.

APPENDIX A3: COMPUTATION OF PERCENTILES

The q-percentile of a continuously given function $f(\boldsymbol{X})$ in the domain with $\boldsymbol{X} \in \Omega_0^A$ is defined by

$$f_q^A : \frac{\int_{\Omega_0^A} \left(I_{(f(\boldsymbol{X})-f_q^A)>0} \right) \mathrm{d}V}{\int_{\Omega_0^A} \mathrm{d}V} = 1 - \frac{q}{100} \tag{44}$$

where $I_{(f(\boldsymbol{X})-f_q^A)>0}$ is the indicator function defined by

$$I_{(\bullet)>0} := \begin{cases} 1, & (\bullet) > 0, \\ 0, & (\bullet) \leq 0 \end{cases}. \tag{45}$$

APPENDIX A4: DETAILED OVERVIEW OF THE PARAMETER STUDY

In the Figures 17, 18, 19, 20, 21 and 22 a detailed overview of the parameter study is given.

TABLE 4 Overview of constitutive models and material parameters of vessel wall, ILT, calcifications and SG. Regarding the notation the reader is referred to the original paper[32].

Vessel wall:[32,25,31,73]

$\Psi^{\text{wall}} = (1-\lambda)\Psi^{\text{AA}} + \lambda\Psi^{\text{AAA}} + \Psi^{\text{calc}}$

$\Psi^{\text{AA}} = c^{\text{AA}}(\bar{I}_1 - 3) + \frac{k_1}{2k_2}\sum_{i=4,6}(e^{k_2[\kappa\bar{I}_1+(1-3\kappa)\bar{I}_i-1]^2} - 1) + \Psi^{\text{AA}}_{\text{vol}}(J)$

$\Psi^{\text{AAA}} = a(\bar{I}_1 - 3) + b(\bar{I}_1 - 3)^2 + \Psi^{\text{AAA}}_{\text{vol}}(J)$

c^{AA} [kPa]: 100.9 k_1 [kPa]: 4070 k_2 [-]: 165.6 κ [-]: 0.16 θ_i [°]: ±48.4

a [kPa]: 174.0 b [kPa]: 1881

Intraluminal thrombus:[32,26]

$\Psi^{\text{ILT}} = c^{\text{ILT}}(\bar{I}_1^2 - 2\bar{I}_2 - 3) + \Psi^{\text{ILT}}_{\text{vol}}(J) + \Psi^{\text{calc}}$

c^{ILT} [kPa]: [1.73; 2.62]

Calcifications:[32,48]

$\Psi^{\text{calc}} = c^{\text{calc}}(\bar{I}_1 - 3) + \Psi^{\text{calc}}_{\text{vol}}(J)$

c^{calc} [kPa]: [0.0; 8929]

Stent:[32,40]

$\Psi^{\text{S}} = \frac{c^{\text{S}}}{\beta^{\text{S}}}(J^{-2\beta^{\text{S}}} - 1) + c^{\text{S}}(I_1 - 3)$

c^{S} [MPa]: 40385 β^{S} [-]: 0.75

Graft:[32,40]

$\Psi^{\text{G}} = \frac{c^{\text{G}}}{\beta^{\text{G}}}(J^{-2\beta^{\text{G}}} - 1) + c^{\text{G}}(I_1 - 3)$

c^{G} [MPa]: 9.45[a] β^{G} [-]: 5.75

[a] reduction of the bending stiffness as described in[75]

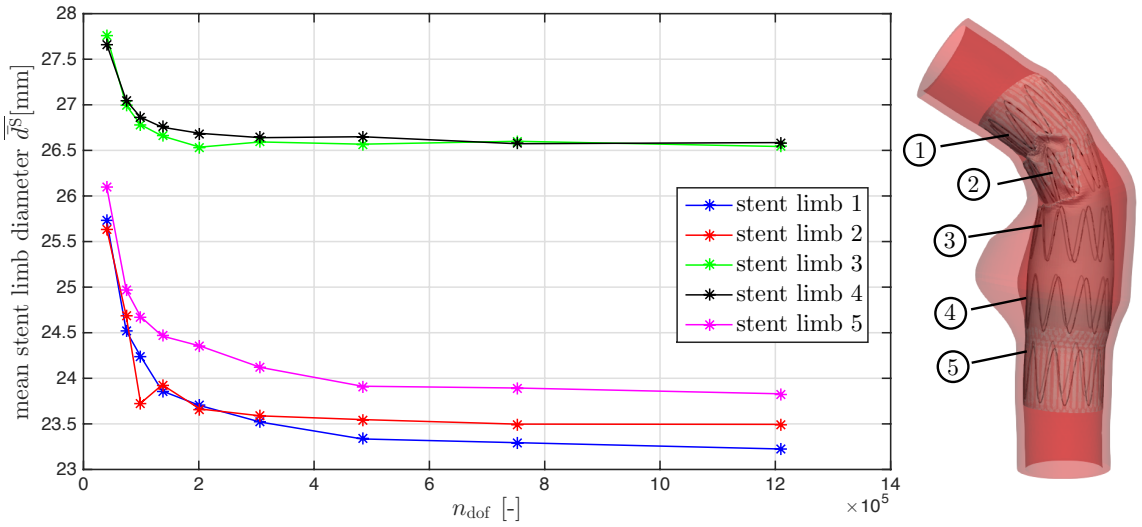

FIGURE 16 Mesh convergence study: mean stent limb diameters $\bar{d}^{\bar{S}}$ of the five stent limbs in the deployed state for different discretizations with the total number of degrees of freedom n_{dof}.

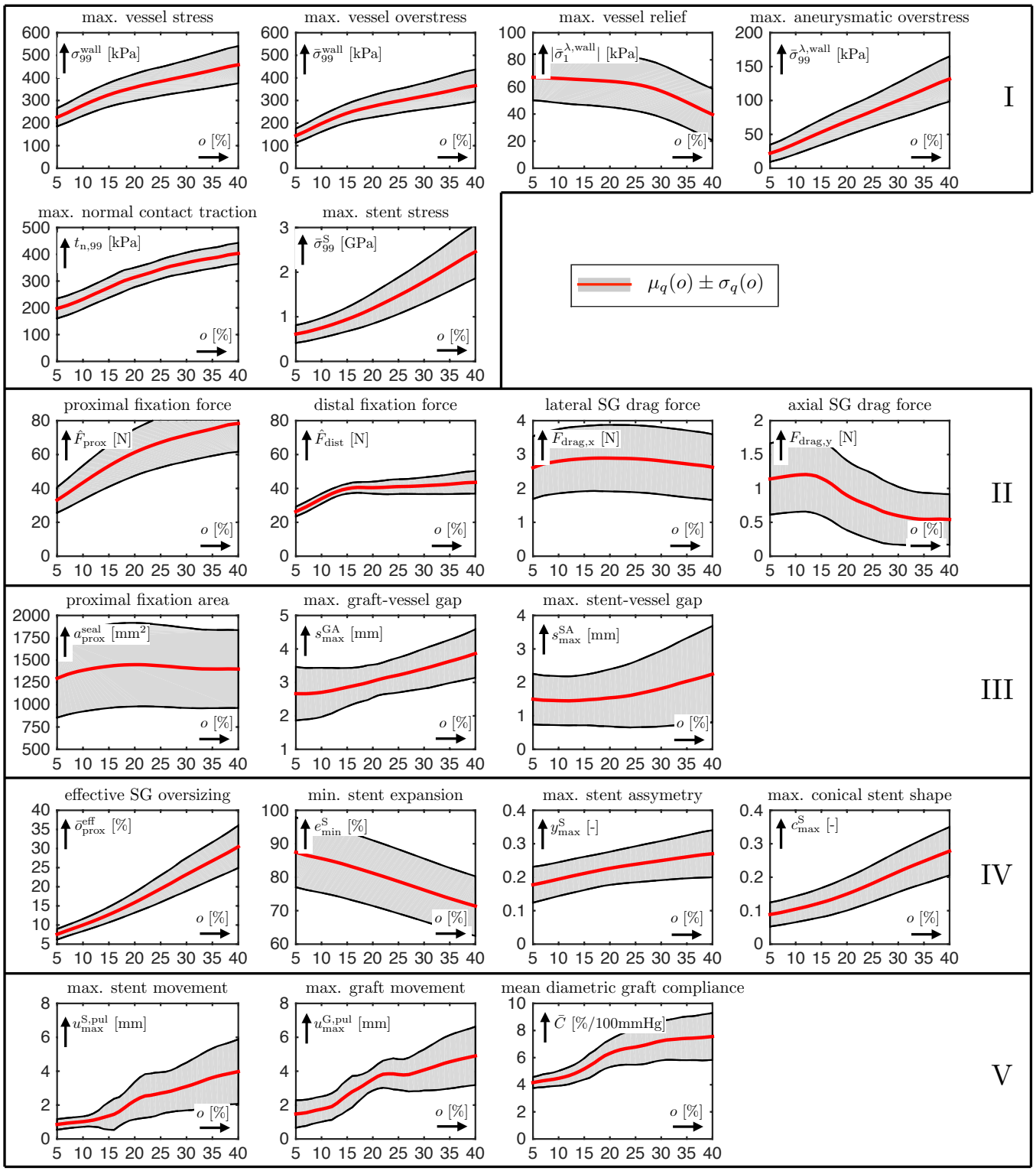

FIGURE 17 Mean±std of all EVAR quality parameters $q \in \mathcal{Q}$ according to equation (36) and (37) depending on the degree of SG oversizing o. The EVAR quality parameters $q \in \mathcal{Q}$ are sorted as they had beed introduced in Section 2.4: vessel and SG stresses and tractions (I), fixation and drag forces (II), quality of seal (III), geometrical parameters of the deployed SG (IV) and parameters depending on the pulsatile blood pressure (V).

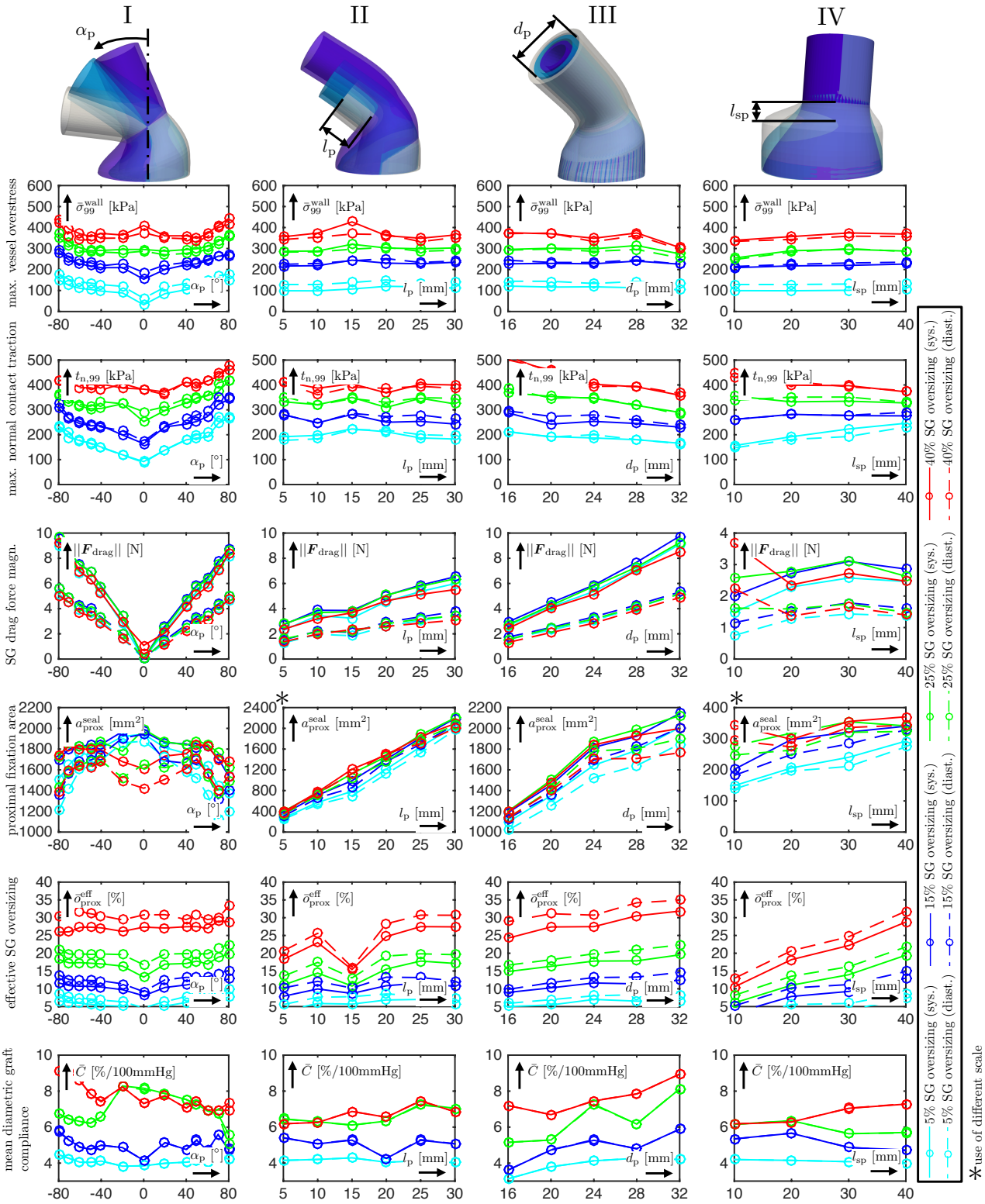

FIGURE 18 Maximum vessel overstress $\bar{\sigma}_{99}^{wall}$, maximum normal contact traction $t_{n,99}$, SG drag force magnitude $||\boldsymbol{F}_{drag}||$, proximal fixation area a_{prox}^{seal}, effective degree of SG oversizing $\bar{o}_{prox}^{eff}$ and mean diametric graft compliance $\bar{C}$ plotted over variations of the proximal neck angle α_p (I), the proximal neck length l_p (II), the proximal neck diameter d_p (III) and the proximal AAA shoulder length l_{sp} (IV) for different degrees of SG oversizing o as well as different blood pressure states $p^{diast} = 80$ mmHg and $p^{sys} = 130$ mmHg.

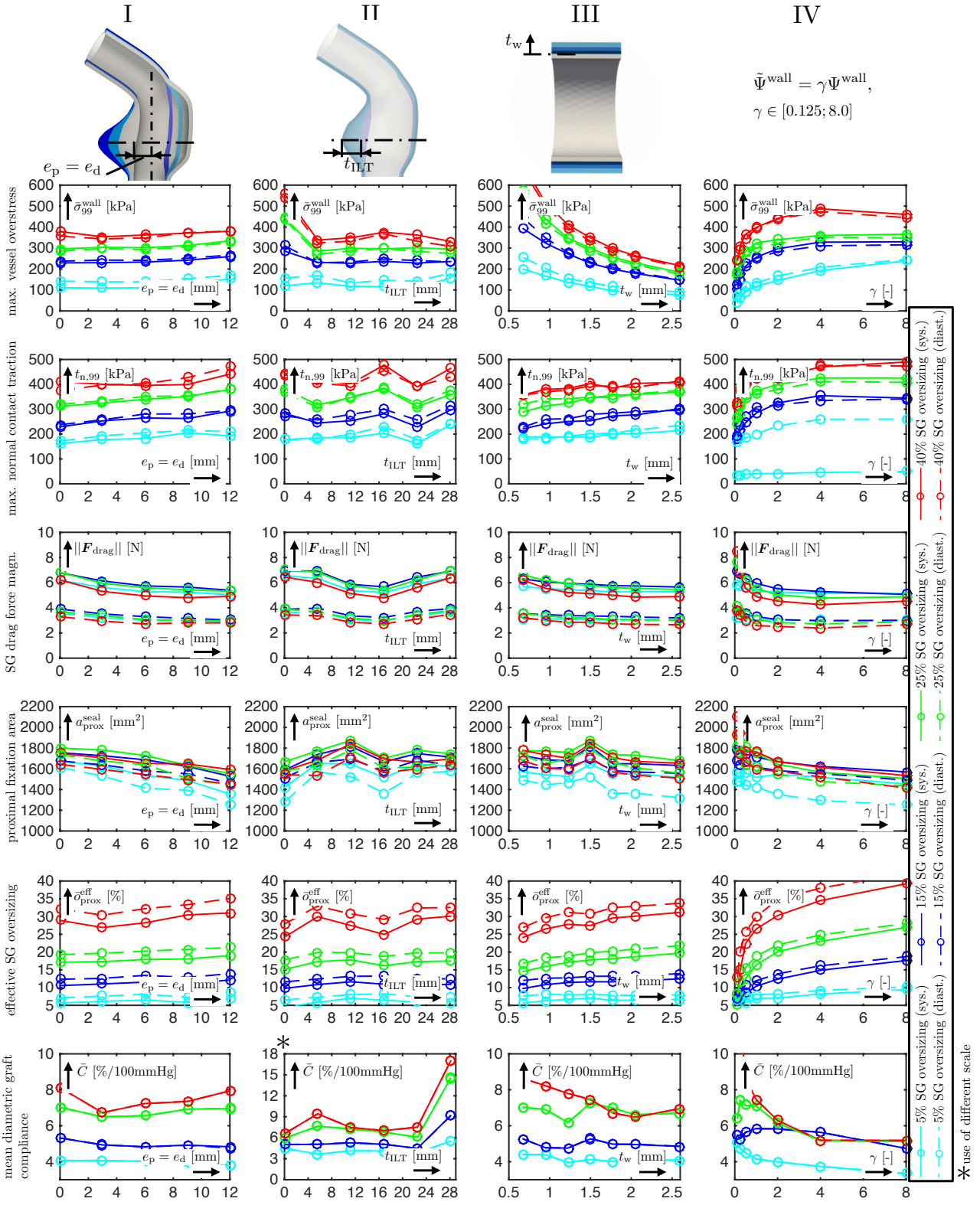

FIGURE 19 Maximum vessel overstress $\bar{\sigma}_{99}^{wall}$, maximum normal contact traction $t_{n,99}$, SG drag force magnitude $||\boldsymbol{F}_{drag}||$, proximal fixation area a_{prox}^{seal}, effective degree of SG oversizing $\bar{o}_{prox}^{eff}$ and mean diametric graft compliance $\bar{C}$ plotted over variations of the aneurysm eccentricity $e_p = e_d$ (I), the ILT thickness t_{ILT} (II), the vessel wall thickness t_w (III) and the vessel wall stiffness γ (IV) for different degrees of SG oversizing o as well as different blood pressure states $p^{diast} = 80$ mmHg and $p^{sys} = 130$ mmHg.

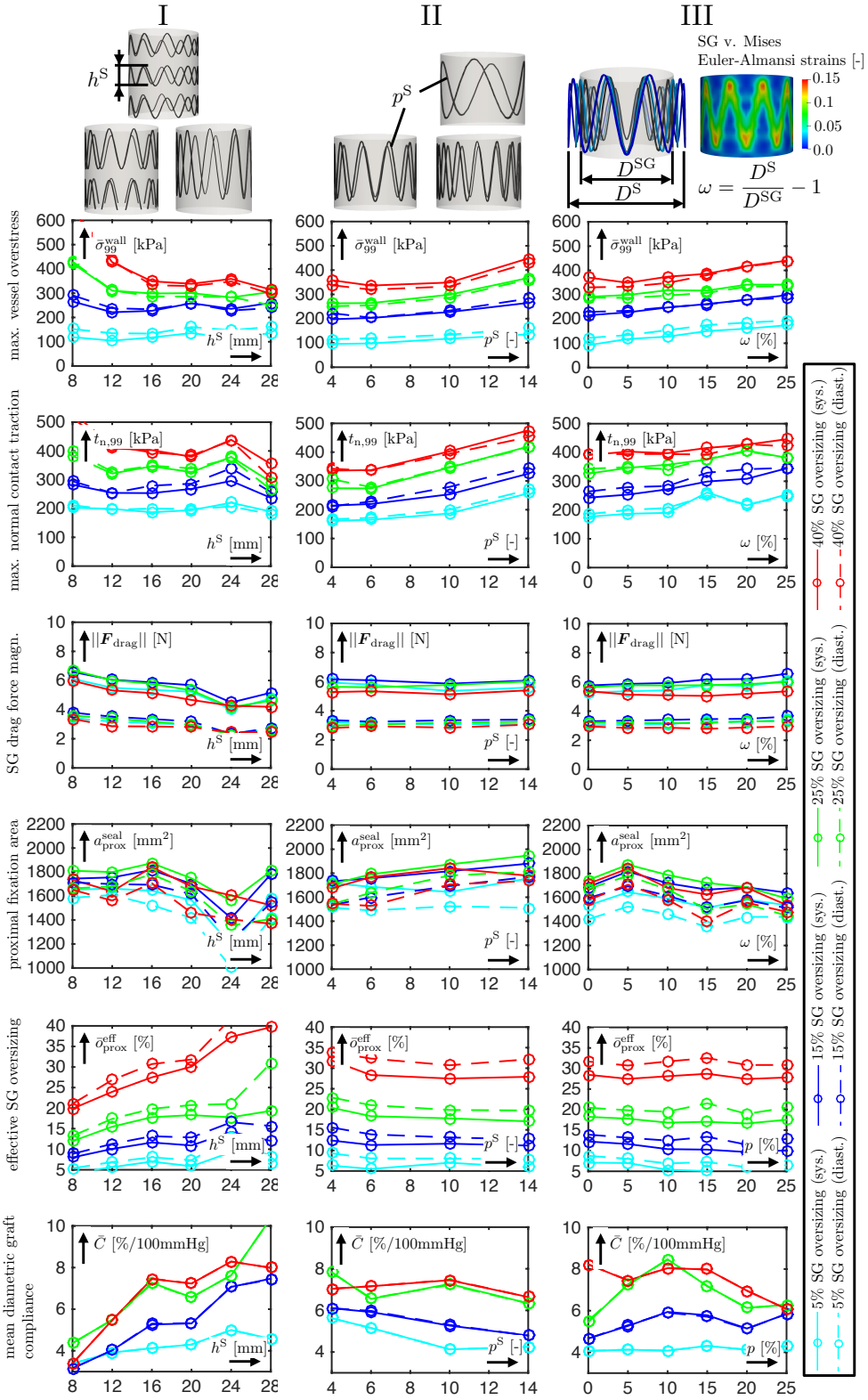

FIGURE 20 Maximum vessel overstress $\bar{\sigma}_{99}^{wall}$, maximum normal contact traction $t_{n,99}$, SG drag force magnitude $||\boldsymbol{F}_{drag}||$, proximal fixation area a_{prox}^{seal}, effective degree of SG oversizing $\bar{o}_{prox}^{eff}$ and mean diametric graft compliance $\bar{C}$ plotted over variations of the stent limb height h^S (I), the number of periods per stent limb p^S (II) and the degree of stent predeformation ω (III) for different degrees of SG oversizing o as well as different blood pressure states $p^{diast} = 80$ mmHg and $p^{sys} = 130$ mmHg.

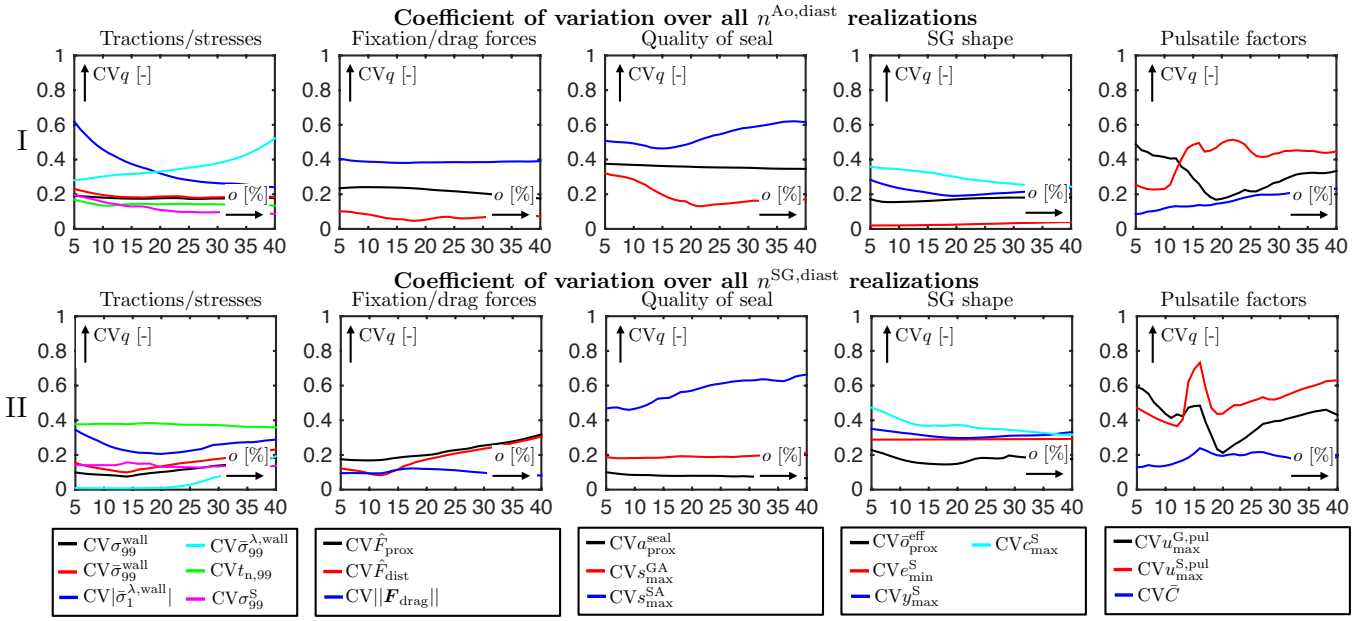

FIGURE 21 Coefficient of variation CVq (equation (35)) over all $n^{\mathrm{Ao,diast}}$ realizations with different vessel geometries (I) as well as over all $n^{\mathrm{SG,diast}}$ realizations with different SG geometries (II) at the diastolic pressure level of $p^{\mathrm{diast}} = 80$ mmHg as a function of the degree of SG oversizing o. CVq is the coefficient of variation of EVAR quality parameter $q \in \mathcal{Q}$. For instance, CV$\sigma_{99}^{\mathrm{wall}}$ is the coefficient of variation of the maximum vessel wall stress $\sigma_{99}^{\mathrm{wall}}$.

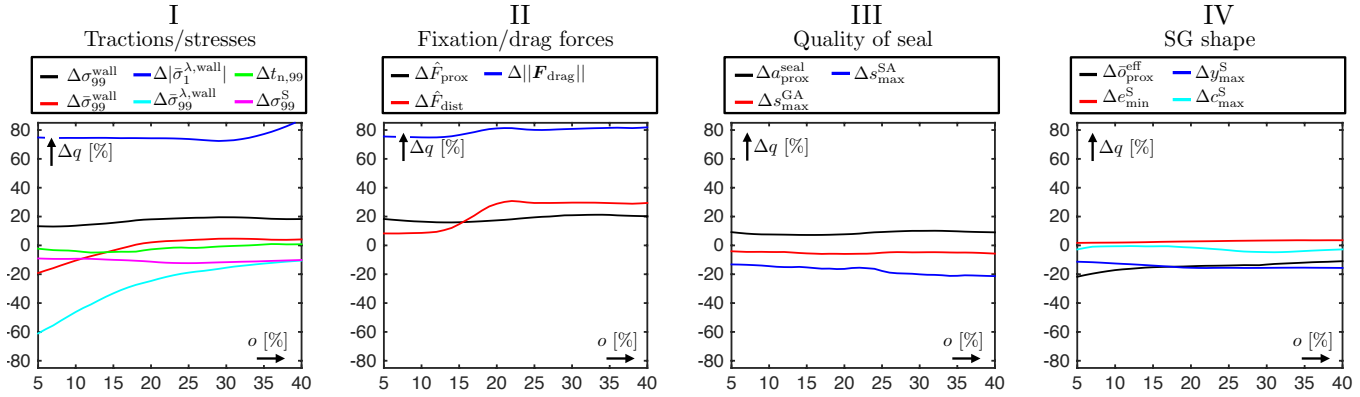

FIGURE 22 Influence of the arterial blood pressure state Δq according to equation (42) on EVAR quality parameters q as a function of the degree of SG oversizing o. Δq describes the relative change of the EVAR quality parameter $q \in \mathcal{Q}$ by a change of the arterial blood pressure from the diastolic state $p^{\mathrm{diast}} = 80$ mmHg to the systolic state $p^{\mathrm{sys}} = 130$ mmHg. For instance, $\Delta\sigma_{99}^{\mathrm{wall}}$ is the relative change of the maximum vessel wall stress $\sigma_{99}^{\mathrm{wall}}$ induced by the blood pressure change.

References

1. A. F. AbuRahma, J. E. Campbell, A. Y. Mousa, S. M. Hass, P. A. Stone, A. Jain, A. Nanjundappa, L. S. Dean, T. Keiffer, and J. Habib, Clinical outcomes for hostile versus favorable aortic neck anatomy in endovascular aortic aneurysm repair using modular devices, *Journal of vascular surgery* **54**, 13–21, 2011.

2. H.-E. Altnji, B. Bou-Saïd, and H. Walter-Le Berre, Morphological and stent design risk factors to prevent migration phenomena for a thoracic aneurysm: a numerical analysis, *Medical engineering and physics* **37**, 23–33, 2015.

3. H.-E. Altnji, B. Bou-Saïd, and H. Walter-Le Berre, Numerical simulation for design evaluation of thoracic stent graft to investigate the migration phenomena and type 1a endoleak of thoracic aneurysm, *J Vasc Med Surg* **3**, 1–7, 2015.

4. G. A. Antoniou, G. S. Georgiadis, S. A. Antoniou, G. Kuhan, and D. Murray, A meta-analysis of outcomes of endovascular abdominal aortic aneurysm repair in patients with hostile and friendly neck anatomy, *Journal of vascular surgery* **57**, 527–538, 2013.

5. F. Auricchio, M. Conti, S. Marconi, A. Reali, J. L. Tolenaar, and S. Trimarchi, Patient-specific aortic endografting simulation: From diagnosis to prediction, *Computers in Biology and Medicine* **43**, 386 – 394, 2013.

6. H. G. Beebe, J. L. Cronenwett, B. T. Katzen, D. C. Brewster, R. M. Green, V. E. T. Investigators, et al., Results of an aortic endograft trial: impact of device failure beyond 12 months, *Journal of vascular surgery* **33**, 55–63, 2001.

7. J. Biehler, M. W. Gee, and W. A. Wall, Towards efficient uncertainty quantification in complex and large-scale biomechanical problems based on a bayesian multi-fidelity scheme, *Biomechanics and modeling in mechanobiology* **14**, 489–513, 2015.

8. F. A. Braeu, A. Seitz, R. C. Aydin, and C. J. Cyron, Homogenized constrained mixture models for anisotropic volumetric growth and remodeling, *Biomechanics and modeling in mechanobiology* **16**, 889–906, 2017.

9. S. Brugaletta, J. Gomez-Lara, R. Diletti, V. Farooq, R. Jan van Geuns, B. de Bruyne, D. Dudek, H. M. Garcia-Garcia, J. A. Ormiston, and P. W. Serruys, Comparison of in vivo eccentricity and symmetry indices between metallic stents and bioresorbable vascular scaffolds: insights from the absorb and spirit trials, *Catheterization and Cardiovascular Interventions* **79**, 219–228, 2012.

10. L. Canaud, P. Alric, M. Laurent, T.-P. Baum, P. Branchereau, C. H. Marty-Ané, and J.-P. Berthet, Proximal fixation of thoracic stent-grafts as a function of oversizing and increasing aortic arch angulation in human cadaveric aortas, *Journal of Endovascular Therapy* **15**, 326–334, 2008.

11. D. Chamié, H. G. Bezerra, G. F. Attizzani, H. Yamamoto, T. Kanaya, G. T. Stefano, Y. Fujino, E. Mehanna, W. Wang, A. Abdul-Aziz, et al., Incidence, predictors, morphological characteristics, and clinical outcomes of stent edge dissections detected by optical coherence tomography, *JACC: Cardiovascular Interventions* **6**, 800–813, 2013.

12. R. W. Chang, P. Goodney, L.-Y. Tucker, S. Okuhn, H. Hua, A. Rhoades, N. Sivamurthy, and B. Hill, Ten-year results of endovascular abdominal aortic aneurysm repair from a large multicenter registry, *Journal of vascular surgery* **58**, 324–332, 2013.

13. D. Chemla, J.-L. Hébert, C. Coirault, K. Zamani, I. Suard, P. Colin, and Y. Lecarpentier, Total arterial compliance estimated by stroke volume-to-aortic pulse pressure ratio in humans, *American Journal of Physiology-Heart and Circulatory Physiology* **274**, H500–H505, 1998.

14. F. Cochennec, J. P. Becquemin, P. Desgranges, E. Allaire, H. Kobeiter, and F. Roudot-Thoraval, Limb graft occlusion following evar: clinical pattern, outcomes and predictive factors of occurrence, *European journal of vascular and endovascular surgery* **34**, 59–65, 2007.

15. T. J. Corbett, A. Callanan, and T. M. McGloughlin, In vitro measurement of the axial migration force on the proximal end of a bifurcated abdominal aortic aneurysm stent-graft model, *Proceedings of the Institution of Mechanical Engineers, Part H: Journal of Engineering in Medicine* **225**, 401–409, 2011.

16. T. Corbett, D. Molony, E. Kavanagh, P. Grace, M. Walsh, and T. McGloughlin, Experimental analysis of endovascular treatment of aaa and predictors of long term outcomes, *Biomechanics and Mechanobiology of Aneurysms*, 247–284, 2011.

17. T. J. Corbett, A. Callanan, L. G. Morris, B. J. Doyle, P. A. Grace, E. G. Kavanagh, and T. M. McGloughlin, A review of the in vivo and in vitro biomechanical behavior and performance of postoperative abdominal aortic aneurysms and implanted stent-grafts, *Journal of Endovascular Therapy* **15**, 468–484, 2008.

18. S. De Bock, F. Iannaccone, M. De Beule, F. Vermassen, P. Segers, and B. Verhegghe, What if you stretch the ifu? a mechanical insight into stent graft instructions for use in angulated proximal aneurysm necks, *Medical engineering and physics* **36**, 1567–1576, 2014.

19. E. de Souza Neto, D. Perić, M. Dutko, and D. Owen, Design of simple low order finite elements for large strain analysis of nearly incompressible solids, *International Journal of Solids and Structures* **33**, 3277–3296, 1996.

20. N. Demanget, A. Duprey, P. Badel, L. Orgéas, S. Avril, C. Geindreau, J.-N. Albertini, and J.-P. Favre, Finite element analysis of the mechanical performances of 8 marketed aortic stent-grafts, *Journal of Endovascular Therapy* **20**, 523–535, 2013.

21. N. Diehm, F. Dick, B. T. Katzen, J. Schmidli, C. Kalka, and I. Baumgartner, Aortic neck dilatation after endovascular abdominal aortic aneurysm repair: a word of caution, *Journal of vascular surgery* **47**, 886–892, 2008.

22. E. D. Dillavou, S. C. Muluk, R. Y. Rhee, E. Tzeng, J. D. Woody, N. Gupta, and M. S. Makaroun, Does hostile neck anatomy preclude successful endovascular aortic aneurysm repair?, *Journal of vascular surgery* **38**, 657–663, 2003.

23. G. Dobson, J. Flewitt, J. V. Tyberg, R. Moore, and M. Karamanoglu, Endografting of the descending thoracic aorta increases ascending aortic input impedance and attenuates pressure transmission in dogs, *European journal of vascular and endovascular surgery* **32**, 129–135, 2006.

24. C. A. Figueroa, C. A. Taylor, V. Yeh, A. J. Chiou, and C. K. Zarins, Effect of curvature on displacement forces acting on aortic endografts: a 3-dimensional computational analysis, *Journal of Endovascular Therapy* **16**, 284–294, 2009.

25. T. C. Gasser, R. W. Ogden, and G. A. Holzapfel, Hyperelastic modelling of arterial layers with distributed collagen fibre orientations, *Journal of the royal society interface* **3**, 15–35, 2006.

26. T. C. Gasser, G. Görgülü, M. Folkesson, and J. Swedenborg, Failure properties of intraluminal thrombus in abdominal aortic aneurysm under static and pulsating mechanical loads, *Journal of vascular surgery* **48**, 179–188, 2008.

27. M. W. Gee, C. Förster, and W. A. Wall, A computational strategy for prestressing patient-specific biomechanical problems under finite deformation, *International Journal for Numerical Methods in Biomedical Engineering* **26**, 52–72, 2010.

28. R. M. Greenhalgh and J. T. Powell, Endovascular repair of abdominal aortic aneurysm, *New England Journal of Medicine* **358**, 494–501, 2008.

29. K. A. Hance, J. Hsu, T. Eskew, and A. S. Hermreck, Secondary aortoesophageal fistula after endoluminal exclusion because of thoracic aortic transection, *Journal of vascular surgery* **37**, 886–888, 2003.

30. S. E. Hardt, A. Just, R. Bekeredjian, W. Kübler, H. R. Kirchheim, and H. F. Kuecherer, Aortic pressure-diameter relationship assessed by intravascular ultrasound: experimental validation in dogs, *American Journal of Physiology-Heart and Circulatory Physiology* **276**, H1078–H1085, 1999.

31. D. Haskett, G. Johnson, A. Zhou, U. Utzinger, and J. V. Geest, Microstructural and biomechanical alterations of the human aorta as a function of age and location, *Biomechanics and modeling in mechanobiology* **9**, 725–736, 2010.

32. A. Hemmler, B. Lutz, C. Reeps, G. Kalender, and M. W. Gee, A methodology for in silico endovascular repair of abdominal aortic aneurysms, *Biomechanics and Modeling in Mechanobiology* **17**, 1139–1164, 2018.

33. A. Hemmler, B. Lutz, G. Kalender, C. Reeps, and M. W. Gee, Patient-specific in silico endovascular repair of abdominal aortic aneurysms: application and validation, *Biomechanics and Modeling in Mechanobiology* **18**, 983–1004, 2019.

34. B. A. Howell, T. Kim, A. Cheer, H. Dwyer, D. Saloner, and T. A. Chuter, Computational fluid dynamics within bifurcated abdominal aortic stent-grafts, *Journal of Endovascular Therapy* **14**, 138–143, 2007.

35. T. S. Jacobs, J. Won, E. C. Gravereaux, P. L. Faries, N. Morrissey, V. J. Teodorescu, L. H. Hollier, and M. L. Marin, Mechanical failure of prosthetic human implants: a 10-year experience with aortic stent graft devices, *Journal of vascular surgery* **37**, 16–26, 2003.

36. R. Jayendiran, B. Nour, and A. Ruimi, Fluid-structure interaction (fsi) analysis of stent-graft for aortic endovascular aneurysm repair (evar): Material and structural considerations, *Journal of the mechanical behavior of biomedical materials* **87**, 95–110, 2018.

37. W. D. Jordan, K. Ouriel, M. Mehta, D. Varnagy, W. M. Moore, F. R. Arko, J. Joye, J.-P. P. de Vries, J. P. de Vries, H. Eckstein, et al., Outcome-based anatomic criteria for defining the hostile aortic neck, *Journal of vascular surgery* **61**, 1383–1390, 2015.

38. H. Kandail, M. Hamady, and X. Y. Xu, Comparison of blood flow in branched and fenestrated stent-grafts for endovascular repair of abdominal aortic aneurysms, *Journal of Endovascular Therapy* **22**, 578–590, 2015.

39. D. E. Kiousis, T. C. Gasser, and G. A. Holzapfel, A numerical model to study the interaction of vascular stents with human atherosclerotic lesions, *Annals of biomedical engineering* **35**, 1857–1869, 2007.

40. C. Kleinstreuer, Z. Li, C. Basciano, S. Seelecke, and M. Farber, Computational mechanics of nitinol stent grafts, *Journal of biomechanics* **41**, 2370–2378, 2008.

41. G. N. Kouvelos, K. Oikonomou, G. A. Antoniou, E. L. Verhoeven, and A. Katsargyris, A systematic review of proximal neck dilatation after endovascular repair for abdominal aortic aneurysm, *Journal of Endovascular Therapy* **24**, 59–67, 2017.

42. J. A. Kratzberg, J. Golzarian, and M. L. Raghavan, Role of graft oversizing in the fixation strength of barbed endovascular grafts, *Journal of vascular surgery* **49**, 1543–1553, 2009.

43. T. Länne, B. Sonesson, D. Bergqvist, H. Bengtsson, and D. Gustafsson, Diameter and compliance in the male human abdominal aorta: influence of age and aortic aneurysm, *European journal of vascular surgery* **6**, 178–184, 1992.

44. J. H. Leung, A. R. Wright, N. Cheshire, J. Crane, S. A. Thom, A. D. Hughes, and Y. Xu, Fluid structure interaction of patient specific abdominal aortic aneurysms: a comparison with solid stress models, *Biomedical engineering online* **5**, 1–15, 2006.

45. Z. Li, C. Kleinstreuer, and M. Farber, Computational analysis of biomechanical contributors to possible endovascular graft failure, *Biomechanics and Modeling in Mechanobiology* **4**, 221–234, 2005.

46. Z. Li and C. Kleinstreuer, Analysis of biomechanical factors affecting stent-graft migration in an abdominal aortic aneurysm model, *Journal of biomechanics* **39**, 2264–2273, 2006.

47. K. Liffman, M. M. Lawrence-Brown, J. B. Semmens, A. Bui, M. Rudman, and D. E. Hartley, Analytical modeling and numerical simulation of forces in an endoluminal graft, *Journal of Endovascular Therapy* **8**, 358–371, 2001.

48. A. Maier, M. W. Gee, C. Reeps, H.-H. Eckstein, and W. A. Wall, Impact of calcifications on patient-specific wall stress analysis of abdominal aortic aneurysms, *Biomechanics and modeling in mechanobiology* **9**, 511–521, 2010.

49. A. Maier, M. W. Gee, C. Reeps, J. Pongratz, H.-H. Eckstein, and W. A. Wall, A comparison of diameter, wall stress, and rupture potential index for abdominal aortic aneurysm rupture risk prediction, *Annals of biomedical engineering* **38**, 3124–3134, 2010.

50. A. Maier, M. Essler, M. W. Gee, H.-H. Eckstein, W. A. Wall, and C. Reeps, Correlation of biomechanics to tissue reaction in aortic aneurysms assessed by finite elements and [18f]–fluorodeoxyglucose–pet/ct, *International journal for numerical methods in biomedical engineering* **28**, 456–471, 2012.

51. R. Makar, J. Reid, A. Pherwani, L. Johnston, R. Hannon, B. Lee, and C. Soong, Aorto-enteric fistula following endovascular repair of abdominal aortic aneurysm, *European Journal of Vascular and Endovascular Surgery* **20**, 588–590, 2000.

52. G. Maleux, M. Koolen, and S. Heye, Complications after endovascular aneurysm repair, *Seminars in interventional radiology* **26**, 3–9, 2009.

53. C. O. McDonnell, M. Halak, A. Bartlett, and S. R. Baker, Abdominal aortic aneurysm neck morphology: proposed classification system, *Irish journal of medical science* **175**, 4–8, 2006.

54. D. J. McGrath, B. O'Brien, M. Bruzzi, N. Kelly, J. Clauser, U. Steinseifer, and P. E. McHugh, Evaluation of cover effects on bare stent mechanical response, *Journal of the mechanical behavior of biomedical materials* **61**, 567–580, 2016.

55. N. Melas, A. Saratzis, N. Saratzis, J. Lazaridis, D. Psaroulis, K. Trygonis, and D. Kiskinis, Aortic and iliac fixation of seven endografts for abdominal-aortic aneurysm repair in an experimental model using human cadaveric aortas, *European Journal of Vascular and Endovascular Surgery* **40**, 429–435, 2010.

56. I. V. Mohan, P. L. Harris, C. J. van Marrewijk, R. J. Laheij, and T. V. How, Factors and forces influencing stent-graft migration after endovascular aortic aneurysm repair, *Journal of Endovascular Therapy* **9**, 748–755, 2002.

57. P. Moireau, N. Xiao, M. Astorino, C. A. Figueroa, D. Chapelle, C. A. Taylor, and J.-F. Gerbeau, External tissue support and fluid–structure simulation in blood flows, *Biomechanics and modeling in mechanobiology* **11**, 1–18, 2012.

58. F. L. Moll, J. Powell, G. Fraedrich, F. Verzini, S. Haulon, M. Waltham, J. Van Herwaarden, P. Holt, J. Van Keulen, B. Rantner, et al., Management of abdominal aortic aneurysms clinical practice guidelines of the european society for vascular surgery, *European Journal of Vascular and Endovascular Surgery* **41**, S1–S58, 2011.

59. D. S. Molony, E. G. Kavanagh, P. Madhavan, M. T. Walsh, and T. M. McGloughlin, A computational study of the magnitude and direction of migration forces in patient-specific abdominal aortic aneurysm stent-grafts, *European journal of vascular and endovascular surgery* **40**, 332–339, 2010.

60. L. Morris, P. Delassus, M. Walsh, and T. McGloughlin, A mathematical model to predict the in vivo pulsatile drag forces acting on bifurcated stent grafts used in endovascular treatment of abdominal aortic aneurysms (aaa), *Journal of biomechanics* **37**, 1087–1095, 2004.

61. L. Morris, F. Stefanov, and T. McGloughlin, Stent graft performance in the treatment of abdominal aortic aneurysms: the influence of compliance and geometry, *Journal of biomechanics* **46**, 383–395, 2013.

62. D. Palombo, D. Valenti, M. Ferri, A. Gaggiano, R. Mazzei, M. Vola, and S. Tettoni, Changes in the proximal neck of abdominal aortic aneurysms early after endovascular treatment, *Annals of vascular surgery* **17**, 408–410, 2003.

63. J. Peidro, M. Boufi, A. D. Loundou, O. Hartung, B. Dona, F. Vernet, D. Bensoussan, and Y. S. Alimi, Aortic anatomy and complications of the proximal sealing zone after endovascular treatment of the thoracic aorta, *Annals of vascular surgery* **48**, 141–150, 2018.

64. D. Perrin, P. Badel, L. Orgéas, C. Geindreau, A. Dumenil, J.-N. Albertini, and S. Avril, Patient-specific numerical simulation of stent-graft deployment: Validation on three clinical cases, *Journal of Biomechanics* **48**, 1868 – 1875, 2015.

65. D. Perrin, N. Demanget, P. Badel, S. Avril, L. Orgéas, C. Geindreau, and J.-N. Albertini, Deployment of stent grafts in curved aneurysmal arteries: toward a predictive numerical tool, *International journal for numerical methods in biomedical engineering* **31**, e02698, 2015.

66. A. Polanczyk, M. Podyma, L. Trebinski, J. Chrzastek, I. Zbicinski, and L. Stefanczyk, A novel attempt to standardize results of cfd simulations basing on spatial configuration of aortic stent-grafts, *PloS one* **11**, e0153332, 2016.

67. A. Polanczyk, A. Piechota-Polanczyk, and L. Stefańczyk, A new approach for the pre-clinical optimization of a spatial configuration of bifurcated endovascular prosthesis placed in abdominal aortic aneurysms, *PloS one* **12**, e0182717, 2017.

68. A. Popp, M. W. Gee, and W. A. Wall, A finite deformation mortar contact formulation using a primal–dual active set strategy, *International Journal for Numerical Methods in Engineering* **79**, 1354–1391, 2009.

69. A. Popp, M. Gitterle, M. W. Gee, and W. A. Wall, A dual mortar approach for 3d finite deformation contact with consistent linearization, *International Journal for Numerical Methods in Engineering* **83**, 1428–1465, 2010.

70. A. Prasad, N. Xiao, X.-Y. Gong, C. K. Zarins, and C. A. Figueroa, A computational framework for investigating the positional stability of aortic endografts, *Biomechanics and modeling in mechanobiology* **12**, 869–887, 2012.

71. B. Y. Rafii, O. J. Abilez, P. Benharash, and C. K. Zarins, Lateral movement of endografts within the aneurysm sac is an indicator of stent-graft instability, *Journal of Endovascular Therapy* **15**, 335–343, 2008.

72. M. L. Raghavan, J. A. Kratzberg, and J. Golzarian, Introduction to biomechanics related to endovascular repair of abdominal aortic aneurysm, *Techniques in Vascular & Interventional Radiology* **8**, 50–55, 2005.

73. M. Raghavan and D. A. Vorp, Toward a biomechanical tool to evaluate rupture potential of abdominal aortic aneurysm: identification of a finite strain constitutive model and evaluation of its applicability, *Journal of Biomechanics* **33**, 475 – 482, 2000.

74. R. M. Romarowski, M. Conti, S. Morganti, V. Grassi, M. Marrocco-Trischitta, S. Trimarchi, and F. Auricchio, Computational simulation of tevar in the ascending aorta for optimal endograft selection: A patient-specific case study, *Computers in biology and medicine* **103**, 140–147, 2018.

75. D. Roy, S. Lerouge, K. Inaekyan, C. Kauffmann, R. Mongrain, and G. Soulez, Experimental validation of more realistic computer models for stent-graft repair of abdominal aortic aneurysms, including pre-load assessment, *International journal for numerical methods in biomedical engineering* **32**, e02769, 2016.

76. S. M. Sampaio, J. M. Panneton, G. I. Mozes, J. C. Andrews, T. C. Bower, M. Karla, A. A. Noel, K. J. Cherry, T. Sullivan, and P. Gloviczki, Proximal type i endoleak after endovascular abdominal aortic aneurysm repair: predictive factors, *Annals of vascular surgery* **18**, 621–628, 2004.

77. S. M. Sampaio, J. M. Panneton, G. Mozes, J. C. Andrews, A. A. Noel, M. Kalra, T. C. Bower, K. J. Cherry, T. M. Sullivan, and P. Gloviczki, Aortic neck dilation after endovascular abdominal aortic aneurysm repair: should oversizing be blamed?, *Annals of vascular surgery* **20**, 338–345, 2006.

78. A. Schanzer, R. K. Greenberg, N. Hevelone, W. P. Robinson, M. H. Eslami, R. J. Goldberg, and L. Messina, Predictors of abdominal aortic aneurysm sac enlargement after endovascular repair, *Circulation* **123**, 2848–2855, 2011.

79. C. Schlensak, T. Doenst, M. Hauer, J. Bitu-Moreno, P. Uhrmeister, G. Spillner, and F. Beyersdorf, Serious complications that require surgical interventions after endoluminal stent-graft placement for the treatment of infrarenal aortic aneurysms, *Journal of vascular surgery* **34**, 198–203, 2001.

80. R. C. Schuurmann, S. P. Overeem, K. van Noort, B. A. de Vries, C. H. Slump, and J.-P. P. de Vries, Validation of a new methodology to determine 3-dimensional endograft apposition, position, and expansion in the aortic neck after endovascular aneurysm repair, *Journal of Endovascular Therapy* **25**, 358–365, 2018.

81. T. Shiraev, N. Agostinho, and S. Dubenec, Sizing considerations for gore excluder in angulated aortic aneurysm necks, *Annals of vascular surgery* **49**, 152–157, 2018.

82. N. Simon-Kupilik, H. Schima, L. Huber, R. Moidl, G. Wipplinger, U. Losert, E. Wolner, and P. Simon, Prosthetic replacement of the aorta is a risk factor for aortic root aneurysm development, *The Annals of thoracic surgery* **73**, 455–459, 2002.

83. C. Singh, X. Wang, Y. Morsi, and C. S. Wong, Importance of stent-graft design for aortic arch aneurysm repair, *AIMS Bioengineering* **4**, 133, 2017.

84. L. Speelman, E. M. H. Bosboom, G. W. H. Schurink, F. A. M. V. I. Hellenthal, J. Buth, M. Breeuwer, M. J. Jacobs, and F. N. van de Vosse, Patient-specific aaa wall stress analysis: 99-percentile versus peak stress, *European Journal of Vascular and Endovascular Surgery* **36**, 668–676, 2008.

85. F. Stefanov, T. McGloughlin, and L. Morris, A computational assessment of the hemodynamic effects of crossed and non-crossed bifurcated stent-graft devices for the treatment of abdominal aortic aneurysms, *Medical engineering & physics* **38**, 1458–1473, 2016.

86. W. C. Sternbergh, S. R. Money, R. K. Greenberg, T. A. Chuter, Z. Investigators, et al., Influence of endograft oversizing on device migration, endoleak, aneurysm shrinkage, and aortic neck dilation: results from the zenith multicenter trial, *Journal of vascular surgery* **39**, 20–26, 2004.

87. V. D. Tzilalis, D. Kamvysis, P. Panagou, I. Kaskarelis, M. K. Lazarides, T. Perdikides, P. Prassopoulos, and H. Boudoulas, Increased pulse wave velocity and arterial hypertension in young patients with thoracic aortic endografts, *Annals of vascular surgery* **26**, 462–467, 2012.

88. J. W. van Keulen, F. L. Moll, and J. A. van Herwaarden, Tips and techniques for optimal stent graft placement in angulated aneurysm necks, *Journal of vascular surgery* **52**, 1081–1086, 2010.

89. J. van Prehn, F. J. V. Schlösser, B. E. Muhs, H. J. M. Verhagen, F. L. Moll, and J. A. van Herwaarden, Oversizing of aortic stent grafts for abdominal aneurysm repair: a systematic review of the benefits and risks, *European Journal of Vascular and Endovascular Surgery* **38**, 42–53, 2009.

90. D. A. Vorp, W. A. Mandarino, M. W. Webster, and J. Gorcsan III, Potential influence of intraluminal thrombus on abdominal aortic aneurysm as assessed by a new non-invasive method, *Cardiovascular Surgery* **4**, 732–739, 1996.

91. L. Vu-Quoc and X. G. Tan, Optimal solid shells for non-linear analyses of multilayer composites. i. statics, *Computer methods in applied mechanics and engineering* **192**, 975–1016, 2003.

92. Y. G. Wolf, B. B. Hill, W. A. Lee, C. M. Corcoran, T. J. Fogarty, and C. K. Zarins, Eccentric stent graft compression: an indicator of insecure proximal fixation of aortic stent graft, *Journal of vascular surgery* **33**, 481–487, 2001.

93. T. R. Wyss, F. Dick, L. C. Brown, and R. M. Greenhalgh, The influence of thrombus, calcification, angulation, and tortuosity of attachment sites on the time to the first graft-related complication after endovascular aneurysm repair, *Journal of vascular surgery* **54**, 965–971, 2011.

94. M. S. Yeoman, B. D. Reddy, H. C. Bowles, P. Zilla, D. Bezuidenhout, and T. Franz, The use of finite element methods and genetic algorithms in search of an optimal fabric reinforced porous graft system, *Annals of biomedical engineering* **37**, 2266–2287, 2009.

95. C. K. Zarins, D. A. Bloch, T. Crabtree, A. H. Matsumoto, R. A. White, and T. J. Fogarty, Stent graft migration after endovascular aneurysm repair: importance of proximal fixation, *Journal of vascular surgery* **38**, 1264–1272, 2003.

96. S. Zeinali-Davarani, A. Sheidaei, and S. Baek, A finite element model of stress-mediated vascular adaptation: application to abdominal aortic aneurysms, *Computer methods in biomechanics and biomedical engineering* **14**, 803–817, 2011.